



This implies that all solutions of (1) exist for  $t \in [0, +\infty)$  and, thus, system (1) generates a dynamical system. For  $0 < r \leq 1$ , the stationary set of system (1) consists of a unique stable equilibrium  $S_0 = (0, 0, 0)$ ; for  $r > 1$  a pair of symmetric equilibria  $S_{\pm} = (\pm\sqrt{b(r-1)}, \pm\sqrt{b(r-1)}, r-1)$  is added to the stationary set, and  $S_0$  turns into a saddle.

**2) Inner estimation of global stability.** For the Lorenz system (1), combining several approaches based on the construction of Lyapunov functions [6, 7, 26] it is possible to prove the following criterion for the absence of self-excited and hidden oscillations (see Figs. 1a, 1b).

**Theorem 1.** *If for parameters of system (1) one of the following cases holds:*

$$2\sigma \leq b, \quad \text{or} \quad \begin{cases} 2\sigma > b, \\ r < r_{\text{gs}} = \frac{(\sigma+b)(b+1)}{\sigma}, \end{cases} \quad (3)$$

*then there are no nontrivial self-excited and hidden oscillations in the phase space of system (1), and any its solution  $(x(t), y(t), z(t))$  tends to the stationary set as  $t \rightarrow +\infty$ .*

Beyond the estimate (3) in Theorem 1, the analysis of global stability and the birth of nontrivial attractors can be performed numerically. It is further known that the separatrix of saddle  $S_0$  can form a homoclinic loop from which unstable cycles can arise and violate the global stability (however, a set of measure zero does not affect the global attraction on a stationary set from a practical point of view). Using the Fishing principle [16–18] for the Lorenz system (1) it is possible to prove the following:

**Theorem 2.** *For  $\sigma$  and  $b$  fixed, there exists  $r = r_{\text{h}} \in (1, +\infty)$  corresponding to the homoclinic orbit of the saddle equilibrium  $S_0$  if and only if  $3\sigma > 2b + 1$ .*

For instance, for the classical values of parameters  $\sigma = 10$ ,  $b = 8/3$  of system (1) it is possible to find numerically the approximate value of such homoclinic bifurcation  $r_{\text{h}} \approx 13.926$ , when two symmetric homoclinic orbits forming a homoclinic butterfly appear (see Fig. 1c). Further increase of the parameter  $r$  leads to the birth of two saddle periodic orbits from each homoclinic orbit [15].

**3) Outer estimation of global stability.** For systems with a global absorbing set and an unstable stationary set, the existence of self-excited attractors is obvious. From a computational perspective this allows one to use a *standard computational procedure*, in which after a transient process, a trajectory, starting from a point of unstable manifold in a neighborhood of equilibrium, reaches a state of oscillation, thus one can easily identify it. System (1) possesses the absorbing set  $\mathcal{B}$  (see Eq. (2)) and for  $\sigma > b + 1$ ,  $r > r_{\text{cr}} = \sigma \frac{(\sigma+b+3)}{\sigma-b-1}$  all equilibria are unstable. Thus, in this case, system (1) has a nontrivial self-excited attractor: if we consider classical values of parameters  $\sigma = 10$ ,  $b = 8/3$ , then for  $r > r_{\text{cr}}$ , e.g. for

$r = 28$ , it is possible to observe the self-excited chaotic attractor with respect to all three equilibria  $S_0, S_{\pm}$  (see Fig. 2c).

**4) Boundary of practical global stability.** The presence of an absorbing set implies the existence of a globally attractor  $\mathcal{A}_{\text{glob}}$ , which contains all local self-excited and hidden attractors, and stationary set. Thus, inside the set  $\mathcal{B}$  it is possible to study numerically the presence of nontrivial self-excited and hidden attractors for parameters  $r, \sigma, b$  not satisfying conditions (3) of global stability, i.e. by fixing  $\sigma$  and  $b$ , and by decreasing  $r$  from  $r_{\text{cr}}$ . For  $\sigma = 10$ ,  $b = 8/3$ , this gives us the following region  $r \in (r_{\text{gs}}, r_{\text{cr}})$ , where  $r_{\text{gs}} \approx 4.64$ ,  $r_{\text{cr}} \approx 24.74$ .

A nontrivial self-excited attractor can be observed numerically for  $24.06 \lesssim r < r_{\text{cr}} \approx 24.74$  (see e.g. [27]). In this case of nontrivial multistability, system (1) possesses a local chaotic attractor  $\mathcal{A}$  which is self-excited with respect to equilibrium  $S_0$  and co-exists with the trivial attractors  $S_{\pm}$  (see Fig. 2b).

**5) Hidden attractor or transient set?** For the Lorenz system (1) it is still an open question [22, p. 14], whether for some parameters there exists a hidden chaotic attractor, i.e. whether it is possible by changing parameters to disconnect the basin of attraction from equilibria  $S_0, S_{\pm}$  (e.g. for the parameters  $\sigma = 10$ ,  $b = \frac{8}{3}$ : if  $r = 28$ , then attractor is connected with  $S_0, S_{\pm}$ ; if  $r = 24.5$ , then attractor is connected with only  $S_0$ ). The current results on the existence of the hidden attractors in the Lorenz system are the following: recently reported hidden attractors in the Lorenz system with  $r < r_{\text{cr}}$  and locally stable equilibria  $S_{\pm}$  turn out to be a *transient chaotic set* (a set in the phase space, which can persist for a long time, but after all collapses), but not a *sustained* hidden chaotic attractor [28, 29].

In a numerical computation of a trajectory over a finite-time interval it is difficult to distinguish a *sustained chaos* from a *transient chaos* [30, 31], thus it is reasonable to give a similar classification for transient chaotic sets [32, 33]: *transient chaotic set* is a *hidden* one if it does not involve and attract trajectories from a small neighborhood of equilibria; otherwise, it is *self-excited*.

For the Lorenz system (1) with parameters  $\sigma = 10$ ,  $b = \frac{8}{3}$  fixed, near the point  $r \approx 24.06$  it is possible to observe a long living transient chaotic set, which is hidden since it's basin of attraction does not intersect with the small vicinities of equilibrium  $S_0$  (see Fig. 2a).

In our experiments, consider system (1) with parameters  $r = 24$ ,  $\sigma = 10$ ,  $b = 8/3$ . Using MATLAB's standard procedure `ode45` with default parameters (relative tolerance  $10^{-3}$ , absolute tolerance  $10^{-6}$ ) for trajectory of system (1) with initial point  $u_0 = (20, 20, 20)$  a transient chaotic behavior is observed on the time interval  $[0, 1.8 \cdot 10^4]$ , for initial point  $u_0 = (-7, 8, 22)$  — on the time interval  $[0, 7.2 \cdot 10^4]$ , for initial point  $u_0 = (2, 2, 2)$  — on the time interval  $[0, 2.26 \cdot 10^5]$ , and for initial point  $u_0 = (0, -0.5, 0.5)$  a transient chaotic behavior contin-

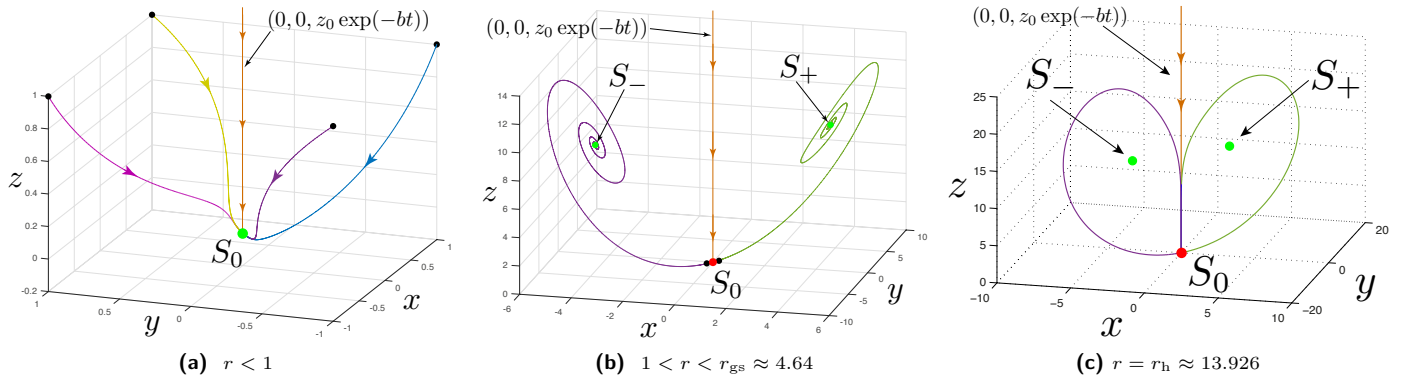


Figure 1: Dynamics of the Lorenz system (1) with fixed parameters  $\sigma = 10$ ,  $b = \frac{8}{3}$ , when parameter  $r$  varying according to the inner estimation of global stability.

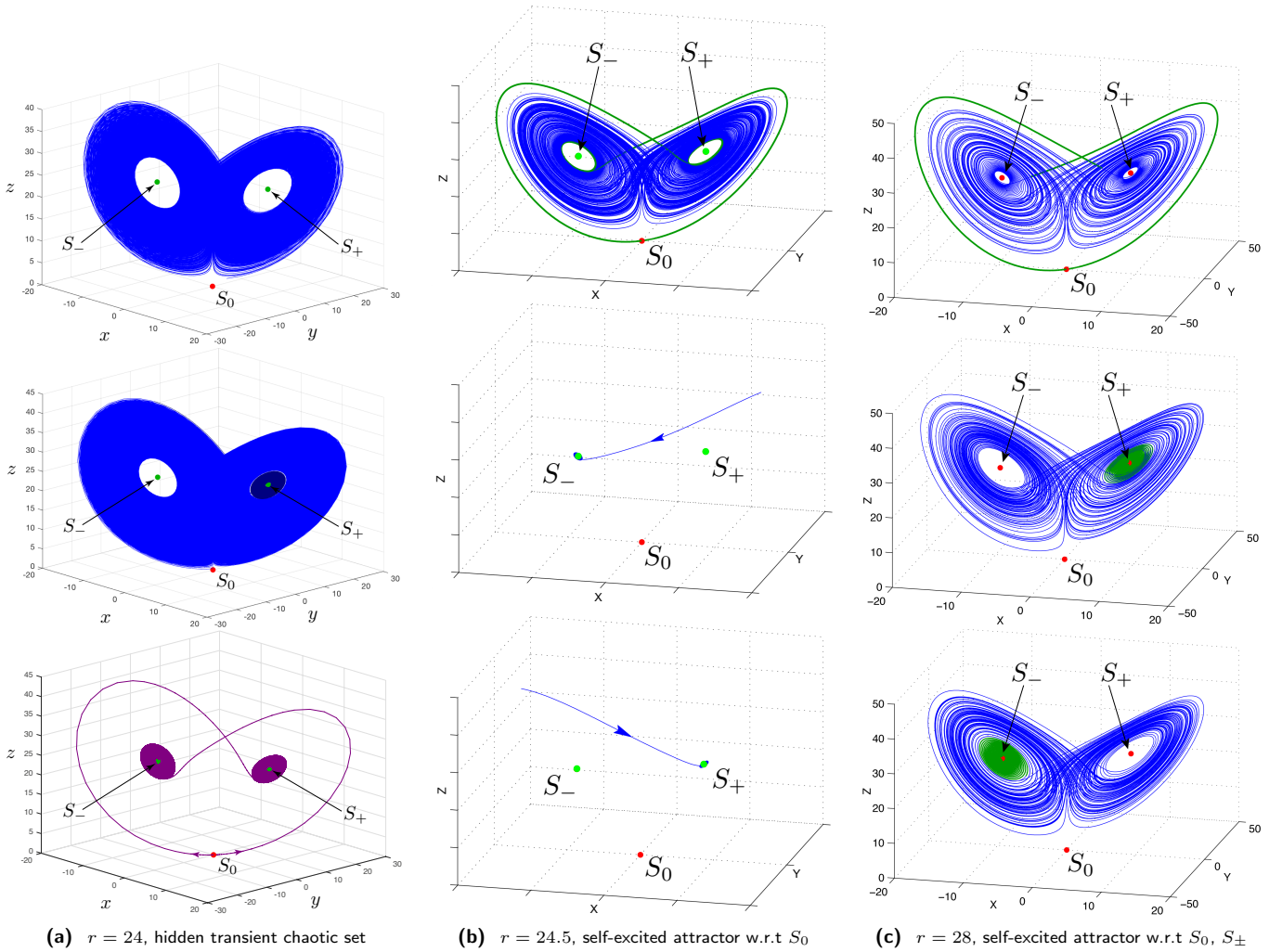


Figure 2: Dynamics of the Lorenz system (1) with fixed parameters  $\sigma = 10$ ,  $b = \frac{8}{3}$ , when parameter  $r$  varying according to the outer estimation of global stability.

ues over a time interval of more than  $[0, 10^7]$ . Remark that, if we consider the same initial points, but use MAT-

LAB's procedure `ode45` with relative tolerance  $10^{-6}$ , for all these initial points the chaotic transient behavior will

last over a time interval of more than  $[0, 10^6]$ , and corresponding transient chaotic sets won't collapse.

## II. THE COMPLEX LORENZ SYSTEM

The classical Lorenz system (1) has gained and still attracts much attention of scientists<sup>3</sup>, however, it is a rather simple mathematical model of the fluid dynamics problem, which E. Lorenz has initially investigated. A more complicated model of many real-world physical problems, such as two-layer baroclinic instability with weak viscosity and beta-effect [34–36] and detuned laser optics [37, 38], is described by the following complex Lorenz system:

$$\begin{cases} \dot{X} = \sigma(Y - X), \\ \dot{Y} = rX - aY - XZ, \\ \dot{Z} = -bZ + \frac{1}{2}(X^*Y + XY^*), \end{cases} \quad (4)$$

where  $X = x_1 + x_2i$ ,  $Y = x_3 + x_4i$  are complex variables,  $Z = x_5$  is real, and " \* " denotes complex conjugation operator. Parameters  $\sigma, b > 0$  are real,  $r = r_1 + r_2i$  and  $a = 1 - ei$  are complex with  $r_1, e \in \mathbb{R}$ . Note that since the transformation  $X \rightarrow X^*, Y \rightarrow Y^*$  changes only the sign of  $r_2$  in (4), this parameter may be chosen positive [39].

System (4) is also dissipative in the sense of Levinson, and the bounded convex absorbing set could be constructed according to the following theorem [40].

**Theorem 3.** *Let for  $\lambda_0 = \min(1, b, \sigma)$  there exist  $\lambda \in (0, \lambda_0)$ ,  $\gamma > 0$ ,  $\vartheta$  such that*

$$\gamma(\sigma - \lambda)(1 - \lambda) - \frac{1}{4} |\sigma + \gamma r - \vartheta|^2 \geq 0. \quad (5)$$

Define  $\Gamma = \frac{\vartheta^2(b-2\lambda)^2}{8\lambda\gamma(b-\lambda)}$ ,  $\beta = \frac{\vartheta^2}{\gamma(1+\gamma)} \left( \frac{(b-2\lambda)^2}{4\lambda(b-\lambda)} + 1 \right)$  and the following function  $W : \mathbb{C} \times \mathbb{C} \times \mathbb{R} \rightarrow \mathbb{R}$ :

$$W(X, Y, Z) = \frac{1}{2} [|X|^2 + \gamma(|Y|^2 + Z^2)] - \vartheta Z.$$

Then for any solution  $(X(t), Y(t), Z(t))$  of (4) and any  $\delta > 0$  with  $T = T(\delta, X(0), Y(0), Z(0))$ , the following inequalities hold for all  $t \geq T$ :

$$W(X(t), Y(t), Z(t)) \leq \Gamma + \delta, \quad (6)$$

and

$$|X(t)|^2 < \beta + \frac{4\delta}{1+\gamma}. \quad (7)$$

Thus, if condition (5) holds, then the solutions of system (4) exist for  $t \in [0, +\infty)$  and, thus, system (4) generates a dynamical system and possesses a global attractor [41] containing a set of all equilibria.

It is also useful to consider the following equivalent form of system (4) in terms of real variables  $x_1, x_2, x_3, x_4, x_5$  and real parameters  $r_1, r_2, \sigma, b, e$  (see, e.g. [39]):

$$\begin{cases} \dot{x}_1 = \sigma(x_3 - x_1), \\ \dot{x}_2 = \sigma(x_4 - x_2), \\ \dot{x}_3 = r_1x_1 - r_2x_2 - x_3 - ex_4 - x_1x_5, \\ \dot{x}_4 = r_2x_1 + r_1x_2 + ex_3 - x_4 - x_2x_5, \\ \dot{x}_5 = -bx_5 + x_1x_3 + x_2x_4. \end{cases} \quad (8)$$

For

$$\text{Im}(r - a) \neq 0, \quad \text{or} \quad \begin{cases} \text{Im}(r - a) = 0, \\ \text{Re}(r - a) \leq 0 \end{cases} \quad (9)$$

system (8) has a unique equilibrium  $S_0 = (0, 0, 0, 0, 0)$ . For

$$\begin{cases} \text{Im}(r - a) = 0, \\ \text{Re}(r - a) > 0 \end{cases} \quad (10)$$

system (8) has a stationary set containing  $S_0$  and a whole circle of equilibria given by the expression:

$$x_1^2 + x_2^2 = b(r_1 - 1), \quad x_1 = x_3, \quad x_2 = x_4, \quad x_5 = r_1 - 1.$$

These equilibria could be parameterized as follows:

$$S_\theta = (\pm\rho \cos(\theta), \pm\rho \sin(\theta), \pm\rho \cos(\theta), \pm\rho \sin(\theta), r_1 - 1),$$

where  $\rho = \sqrt{b(r_1 - 1)}$  and  $\theta \in [0, 2\pi)$ . In literature, relation  $\text{Im}(r - a) = 0$  is often called the "laser case", since in this case system (4) describe the dynamics of some lasers, e.g. a detuned laser [37, 39].

Let us outline the following statements about local stability of the stationary set of system (8) (see e.g. [35]).

**Lemma 1.** *The equilibrium  $S_0$  of system (8) is stable if and only if the following condition hold:*

$$r_1 < r_{1c}, \quad \text{where} \quad r_{1c} = 1 + \frac{(e+r_2)(e-\sigma r_2)}{(\sigma+1)^2}.$$

**Lemma 2.** *The equilibria  $S_\theta$  of system (8) are stable<sup>4</sup> if and only if one of the following conditions hold:*

$$\sigma < b + 1, \quad \text{or} \quad \begin{cases} \sigma > b + 1, \\ 1 < r_1 < r'_{1c} = 1 + \frac{\sqrt{Q_2^2 + 4Q_1Q_3} - Q_2}{2bQ_1}, \end{cases}$$

where

$$\begin{aligned} Q_1 &= (3\sigma + 1)(\sigma - b - 1), \\ Q_2 &= \gamma_2(b + 2\gamma_2)(-2b\gamma_2 - b\gamma_3 + 2\gamma_2\gamma_3) \\ &\quad - \gamma_1(b^2 + b\gamma_2 - b\gamma_3 + 2\gamma_2^2 + 2\gamma_2\gamma_3), \\ Q_3 &= 2\gamma_1\gamma_2 b(b^2 + 2b\gamma_2 + \gamma_1), \end{aligned}$$

and  $\gamma_1 = (\sigma + 1)^2 + \left(\frac{2\sigma(e+r_2)}{\sigma+1} - e\right)^2$ ,  $\gamma_2 = \sigma + 1$ ,  $\gamma_3 = 2\sigma$ .

<sup>3</sup> The original celebrated work by Lorenz [24] has gained more than 24000 cites according to Google Scholar.

<sup>4</sup> One could easily check that the eigenvalues of the Jacobi matrix at all equilibria  $S_\theta$  are the same for any  $\theta \in [0, 2\pi)$ .

### III. INNER ESTIMATION: THE GLOBAL STABILITY AND TRIVIAL ATTRACTORS

Constructing complex-valued Lyapunov functions, by analogy with Theorem 1, it is possible to derive the following criterion for the absence of self-excited and hidden oscillations in the complex Lorenz system (4).

**Theorem 4.** *If for parameters of the system (4) one of the following conditions holds:*

- 1)  $|r+1| < 2$ ,
- 2)  $4r_1 < -r_2^2$ ,
- 3)  $2\sigma - b \neq 0$  and conditions (10) hold. If  $2\sigma - b > 0$ , then for  $\lambda_0 = \min(1, b, \sigma)$ , there exist  $\lambda \in (0, \lambda_0)$ ,  $\gamma > 0$ ,  $\vartheta$ , such that condition on dissipativity (5) and the following inequality hold:

$$\frac{\vartheta^2}{\gamma(1+\gamma)} \left( \frac{(b-2\lambda)^2}{4\lambda(b-\lambda)} + 1 \right) < \frac{b^2(\sigma+1)}{2\sigma-b}. \quad (11)$$

Then in the phase space of system (4), there are no non-trivial self-excited and hidden oscillations, and any of its solution  $(X(t), Y(t), Z(t))$  tends to the stationary set as  $t \rightarrow \infty$ .

*Proof.* We consider the following cases:

**Case 1.** For  $|r+1| < 2$ , one can check that conditions (9) are satisfied and in this case  $S_0$  is the only equilibria of system (4). So, the absence of self-excited oscillations follows from the Routh-Hurwitz criterion on local stability for the equilibrium  $S_0$ . The absence of hidden oscillations can be obtained by Barbashin-Krasovskii theorem (see e.g. [6, 9]) and the Lyapunov function, if  $|r+1| < 2$ , from Theorem 3 for  $\vartheta := 0$  and  $\gamma := \sigma$  we get the following Lyapunov function:

$$V(X, Y, Z) = \frac{1}{2}[|X|^2 + \sigma(|Y|^2 + Z^2)]$$

with  $\lambda_0 = \min(1, b, \sigma)$ ,  $\lambda \in (0, \lambda_0)$ ,  $\delta > 0$  and the inequalities  $\sigma(\sigma - \lambda)(1 - \lambda) - \frac{1}{4}\sigma^2 |r+1|^2 \geq 0$  and  $|X(t)|^2 < \frac{4\delta}{1+\sigma}$  hold. The derivative of  $V$  with respect to system (4) is as follows [40]:

$$\dot{V}(X, Y, Z) \leq -\lambda[|X|^2 + \sigma|Y|^2] < 0, \quad \forall X, Y, Z \neq 0.$$

Also,  $V(X, Y, Z) \geq 0$ ,  $V(0, 0, 0) = 0$  and  $V(X, Y, Z) \rightarrow \infty$  as  $|X, Y, Z| \rightarrow \infty$ ; thus, all conditions of Barbashin-Krasovskii theorem are satisfied implying global stability of the unique equilibrium  $S_0$ .

**Case 2.** For  $4r_1 < -r_2^2$ , conditions (9) are also fulfilled and for this case we introduce the following Lyapunov function (see, [39]):

$$V(X, Y, Z) = \frac{1}{2}[D^2|X|^2 + |Y|^2 + Z^2], \quad (12)$$

where  $D = \sqrt{\frac{-r_1}{\sigma}}$ . It is clear that Lyapunov function (12) is positive definite. Rewrite Lyapunov function (12) in terms of real variables:

$$V(x_1, x_2, x_3, x_4, x_5) = \frac{1}{2}[D^2(x_1^2 + x_2^2) + x_3^2 + x_4^2 + x_5^2]. \quad (13)$$

The derivative of  $V$  with respect to system (8) reads:

$$\dot{V} = -\sigma D^2(x_1^2 + x_2^2) - (x_3^2 + x_4^2) - r_2(x_2x_3 - x_1x_4) - bx_5^2. \quad (14)$$

By using the following scaled variables  $(u_1, u_2, u_3, u_4, u_5)$  as:  $x_1 = \frac{u_1}{D\sqrt{\sigma}}$ ,  $x_2 = \frac{u_2}{D\sqrt{\sigma}}$ ,  $x_3 = u_3$ ,  $x_4 = u_4$ ,  $x_5 = \frac{u_5}{\sqrt{b}}$ , we have

$$\dot{V} = -(u_1^2 + u_2^2 + u_3^2 + u_4^2 + u_5^2) - 2\Delta(u_2u_3 - u_1u_4), \quad (15)$$

where  $\Delta = \frac{r_2}{2D\sqrt{\sigma}}$ .

The transformation  $u \rightarrow v$ ,  $u = Av$  with

$$A = \frac{1}{\sqrt{2}} \begin{pmatrix} 0 & -1 & 0 & 1 & 0 \\ 0 & 0 & 1 & 0 & -1 \\ 0 & 0 & 1 & 0 & 1 \\ 0 & 1 & 0 & 1 & 0 \\ \sqrt{2} & 0 & 0 & 0 & 0 \end{pmatrix},$$

leads to the following expression:

$$\dot{V} = -v_1^2 - (1 + \Delta)(v_2^2 + v_3^2) - (1 - \Delta)(v_4^2 + v_5^2).$$

One can see that initial assumption  $4r_1 < -r_2^2$  implies  $\Delta^2 < 1$  and, therefore,  $\dot{V} < 0$ , and all conditions of Barbashin-Krasovskii theorem are satisfied. Thus, the equilibrium  $S_0$  is globally stable.

As we discussed earlier, if conditions (9) are not satisfied, system (4) has a stationary set containing a continuum of equilibria, i.e the zero equilibrium  $S_0$  and the equilibria  $S_\theta$ . In this case, the Barbashin-Krasovskii theorem is not applicable.

**Case 3.** Suppose conditions (10) are satisfied, then the absence of nontrivial oscillations (and, thus, the global stability of the stationary set  $\{S_0, S_\theta\}$ ) can be demonstrated (see, [40]) by the LaSalle principal [7]. For this purpose, consider the following time and coordinate transformations:

$$\begin{cases} t \rightarrow \tau, & \psi : (X, Y, Z) \rightarrow (\chi, \eta, \xi), \\ \tau = \frac{\sqrt{\sigma}}{\varepsilon} t, & \chi = \frac{\varepsilon}{\sqrt{2\sigma}} X, \quad \eta = \frac{\varepsilon^2}{\sqrt{2}} (Y - X), \\ \xi = \varepsilon^2 (Z - \frac{|X|^2}{b}), & \varepsilon = \frac{1}{\sqrt{r-a}} > 0. \end{cases} \quad (16)$$

System (4) transform into the following system:

$$\begin{cases} \dot{\chi} = \frac{d\chi}{d\tau} = \eta, \\ \dot{\eta} = \frac{d\eta}{d\tau} = -\varrho\eta - \xi\chi - \varphi(\chi), \\ \dot{\xi} = \frac{d\xi}{d\tau} = -\kappa\xi - \frac{\Lambda}{2}(\chi^*\eta + \chi\eta^*), \end{cases} \quad (17)$$

where  $\varrho = \frac{\varepsilon(a+\sigma)}{\sqrt{\sigma}}$ ,  $\varphi(\chi) = -\chi + \Theta\chi|\chi|^2$ ,  $\Theta = \frac{2\sigma}{b}$ ,  $\kappa = \frac{\varepsilon b}{\sqrt{\sigma}}$ ,  $\Lambda = \frac{2}{b}(2\sigma - b)$ . Here, the variables  $\chi$  and  $\eta$  are complex while  $\xi$  is real. The new parameters  $\Theta$ ,  $\kappa$ , and  $\Lambda$  are real with  $\Theta > 0$ ,  $\kappa > 0$ , and  $\varrho$  is complex. Consider the following Lyapunov function:

$$V(\chi, \eta, \xi) = \frac{1}{2} \left[ \frac{1}{|\Lambda|} \xi^2 + |\eta|^2 - |\chi|^2 + \frac{\Theta}{2} |\chi|^4 \right]. \quad (18)$$

Note that, the LaSalle principle requires the compactness of the set, where the Lyapunov function  $V$  is defined to show its boundedness from below. In our case, one can show that the inequality  $V(\chi, \eta, \xi) > -\frac{1}{4\Theta}$  is valid for any  $(\chi, \eta, \xi) \in \mathbb{C} \times \mathbb{C} \times \mathbb{R}$ .

From the relation  $\dot{V}(\chi, \eta, \xi) = 0$ , it follows that the largest invariant set

$$M \subset \{(\chi, \eta, \xi) \in \mathbb{C} \times \mathbb{C} \times \mathbb{R} \mid \dot{V}(\chi, \eta, \xi) = 0\}$$

consists of the equilibrium points of system (17).

The derivative of function  $V$  with respect to system (17) is as follows:

$$\begin{aligned} \dot{V}(\chi, \eta, \xi) = & -\frac{\kappa}{|\Lambda|}\xi^2 - \frac{1}{2}(\text{sgn}(\Lambda) + 1)\chi\xi\eta^* \\ & - \frac{1}{2}(\text{sgn}(\Lambda) + 1)\chi^*\xi\eta - \text{Re}\varrho|\eta|^2. \end{aligned} \quad (19)$$

The last thing to check is that  $\dot{V}(\chi, \eta, \xi) \leq 0, \forall \chi, \eta \in \mathbb{C}, \xi \in \mathbb{R}$ . Consider two cases.

**3.1.** If  $\Lambda = 2\sigma - b > 0$ , then following [40] and using Theorem 3, there exist  $\epsilon > 0$  such that for any solution  $(\chi(\tau), \eta(\tau), \xi(\tau))$  of (17) with  $t_0 = t_0(\chi(0), \eta(0), \xi(0))$  the following inequality:

$$|\chi(t)|^2 \leq \frac{\kappa}{\Lambda} \text{Re}\varrho - \epsilon, \quad (20)$$

holds for all  $t \geq t_0$ .

From relations (16) we have  $X(t) = \frac{\sqrt{2\sigma}}{\epsilon}\chi(t)$ , and taking into account (7) we get:

$$|\chi(t)|^2 < \frac{\epsilon^2\beta}{2\sigma} + \frac{2\delta\epsilon^2}{\sigma(1+\gamma)} \quad \forall t \geq t_0. \quad (21)$$

It is easy to check that condition (11) with (21) and using the following constant in Theorem 3:

$$\vartheta = \frac{\pm 2\sqrt{2\gamma\lambda(2\sigma-b)(b-\lambda)[b^2\sigma(\gamma+1)(\sigma+1)+\epsilon(b-2\sigma)(\sigma(\gamma+1)+2\epsilon\delta)]}}{\epsilon b(2\sigma-b)},$$

implies (20).

If  $\Lambda > 0$ , then expression (19) reads as follows:

$$\dot{V}(\chi, \eta, \xi) = -\frac{\kappa}{|\Lambda|}\xi^2 - \chi\xi\eta^* - \chi^*\xi\eta - \text{Re}\varrho|\eta|^2. \quad (22)$$

Since  $\kappa > 0$  and  $\text{Re}\varrho = \frac{\epsilon(1+\sigma)}{\sqrt{\sigma}} > 0$  (see relation (20)), Eq. (22) can be written as follows:

$$\dot{V}(\chi, \eta, \xi) \leq -\delta_1(\xi^2 + |\eta|^2) \leq 0, \quad \delta_1 > 0. \quad (23)$$

**3.2.** If  $\Lambda < 0$ , then the mixed products in (19) do not appear. Hence, expression (19) can be written immediately in the form (23).

Then, according to LaSalle principle any solution of system (17) (and thus system (4)) tends to an equilibrium state as  $\tau \rightarrow \infty$ .  $\square$

**Remark 1.** For some values of parameters of the complex Lorenz system (4), one can find similar conditions on the global stability as for the Lorenz system (1). For instance, if  $|r+1| < 2$ ,  $S_0$  of the system (4) is globally stable, and choosing  $r_2 = 0$  we obtain  $r_1 < 1$  that corresponds to the condition of global stability of zero equilibrium point of system (1) (see Theorem 1).

**Remark 2.** In the special case, when  $r_2 = e = 0$ , the remaining parameters in the complex Lorenz system (4) are the same as the parameters of the real one (1). However, we can not strictly deduce the condition of global stability of the stationary set  $\{S_0, S_{\pm}\}$  of the Lorenz system (1) from the conditions of Theorem 4. This due to the different behavior of these two systems in this case. The complex Lorenz system (4) still has a continuum of equilibria  $S_{\theta}$  in its phase space, while the real one has only two symmetric equilibria  $S_{\pm}$ . Remark that, for the complex Lorenz system (4) when  $2\sigma \neq b$ , we can only apply the LaSalle principle, and yet it is not possible to apply the Leonov approach [42–44]. While for the real Lorenz system (1), if  $2\sigma < b$ , we can use the LaSalle principle, and if  $2\sigma > b$ , we can apply the Leonov approach [1]. It is also possible to prove global stability, when in system (1) we have  $2\sigma = b$  [1, 45].

Note also that, if in the third condition of Theorem 4 we take the parameters  $\lambda, \gamma, \vartheta$  as follows:  $\gamma = \sigma, \vartheta = \sigma + \sigma r_1 - 2\sigma\sqrt{r_1}, \lambda \in (0, b)$  with  $b \in (0, 1]$ , then we get the following relations between the conditions of global stability for systems (1) and (4):

$$\begin{aligned} r < r_{gs} &= \frac{(\sigma+b)(1+b)}{\sigma} \quad \text{for system (1),} \\ r_1 < r_{1gs} &= \frac{(\sigma-\lambda)(1-\lambda)}{\sigma} \quad \text{for system (4).} \end{aligned}$$

The case, corresponding to condition 3) of Theorem 4, when all trajectories tend to the stationary set, however, not all equilibria of the stationary set are locally stable, is illustrated in Fig. 3.

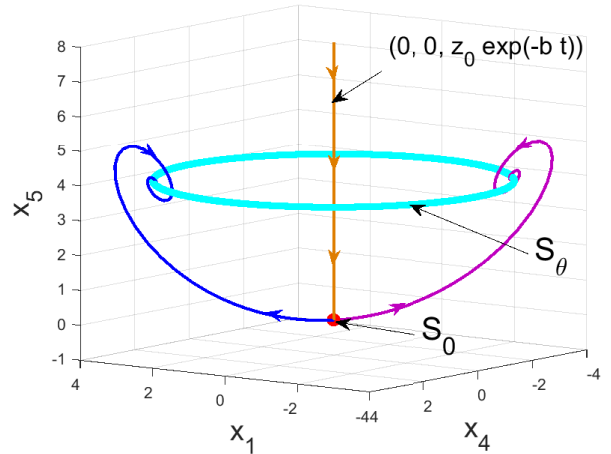


Figure 3: The absence of self-excited and hidden attractors and the global stability of the stationary set  $\{S_0, S_{\theta}\}$  in the system (8) with parameters  $\sigma = 4, r_1 = 5, r_2 = -e = 0.001, b = 4$ . Trajectories (blue, purple) in a small vicinity of the unstable equilibrium  $S_0$  tend to the stable set of equilibria  $S_{\theta}$  (trivial attractors).

**Remark 3.** One of the significant differences between the complex Lorenz (4) and the real one is the following:

in the case when  $S_0$  is the only equilibria of system (4), there could exist a nontrivial attractor, that is a stable limit cycle or even a torus (see Fig. 4).

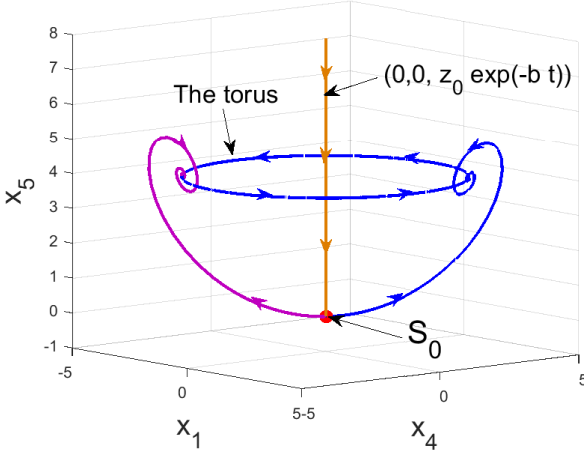


Figure 4: Co-existence of a nontrivial attractive torus and the unstable equilibria  $S_0$  in the system (8) with parameters  $\sigma = 4, r_1 = 5, r_2 = 0.002, e = -0.001, b = 4$ . Trajectories (blue, purple) in small neighborhoods of the unstable equilibrium  $S_0$  attractors to the torus (nontrivial attractors).

Beyond the conditions of Theorem 4, the analysis of global stability and the birth of nontrivial attractors in system (4) can be carried out numerically. For the convenience of this analysis, additional transformations taking into account the structure of a complex system may be useful [46, 47]. For instance, in [48, 49], Vladimirov et. al introduced the following transformation for system (4). If the conditions:

$$2\sigma > b, \quad \sigma(r_1 - 1) - \frac{e^2}{4} \equiv \eta > 0 \quad (24)$$

are satisfied, then using the time and coordinate transformations:

$$\begin{cases} t \rightarrow t', & \psi : (X, Y, Z) \rightarrow (X', Y', Z'), \\ t' = \sqrt{\eta}t, & X' = \eta^{-\frac{3}{4}} \delta X, \quad Y' = \eta^{-\frac{5}{4}} \sigma \delta [Y - (1 + i\delta/2\sigma)X], \\ Z' = \eta^{-1} \sigma (Z - XX^*/2), & \delta = \exp(iet/2) [(2\sigma - b)/2]^{\frac{1}{2}}. \end{cases} \quad (25)$$

one can re-write system (4) in the form:

$$\begin{cases} \frac{dX'}{dt'} = Y', \\ \frac{dY'}{dt'} = (1 + i\kappa)X' - \mu Y' - X'Z' - \varrho X'|X'|^2, \\ \frac{dZ'}{dt'} = -\beta Z' + |X'|^2 \end{cases} \quad (26)$$

where  $\kappa = \frac{(2\sigma r_2 + e(\sigma - 1))}{2\eta}$ ,  $\mu = \frac{1 + \sigma}{\sqrt{\eta}}$ ,  $\varrho = \frac{\sqrt{\eta}}{2\sigma - b}$ ,  $\beta = \frac{b}{\sqrt{\eta}}$ . Since the transformation (25) is continuous and invertible then its a diffeomorphism, and the dynamical behavior of systems (4) and (26) are topologically equivalent [48, 49]. Next, introduce the following real variables  $\xi', v', w', Z'$ :

$$\xi' = (|X'|^2 - |Y'|^2)/2, \quad v' + iw' = X'^* Y'. \quad (27)$$

Expression (27) defines the projection map:  $\Pi : \mathcal{H} \rightarrow \mathcal{P}$ . This map projects all states  $(X', Y', Z')$  in the phase space  $\mathcal{H} = \mathbb{C} \times \mathbb{C} \times \mathbb{R}$  of system (26) (and system (4)), which are invariant with respect to a common phase factor  $\psi$  in  $X'$  and  $Y'$ , i.e.

$$\begin{pmatrix} X' \\ Y' \\ Z' \end{pmatrix} \rightarrow \begin{pmatrix} X' \exp(i\psi) \\ Y' \exp(i\psi) \\ Z' \end{pmatrix}, \quad (28)$$

into the same point  $(\xi', v', w', Z')$  in  $\mathcal{P} = \mathbb{R}^4$ . Indeed, if  $X'' = X' \exp(i\psi)$  and  $Y'' = Y' \exp(i\psi)$ , then

$$\begin{aligned} \xi'' &= (|X''|^2 - |Y''|^2)/2 = (|\exp(i\psi)|^2 [|X'|^2 - |Y'|^2])/2 \\ &= ((\cos^2(\psi) + \sin^2(\psi)) [|X'|^2 - |Y'|^2])/2 \\ &= (|X'|^2 - |Y'|^2)/2 = \xi', \\ v'' + iw'' &= X''^* Y'' = X'^* \exp(-i\psi) Y' \exp(i\psi) \\ &= X'^* Y' = v' + iw'. \end{aligned}$$

As mentioned in [48, 49], the set of points in  $\mathcal{H}$  corresponding to the same point in  $\mathcal{P}$  in geometry is called a "ray", and the space  $\mathcal{P}$  is called a "ray space".

The derivative of expressions (27) with respect to the dynamics of system (26) leads to the following equations of motion in the projective space  $(\xi', v', w', Z') \in \mathcal{P}$ :

$$\begin{cases} \dot{\xi}' = v' + \mu(R - \xi') - \kappa w' - v'(1 - Z' - \varrho(R + \xi')), \\ \dot{v}' = -\mu v' + R - \xi' + (R + \xi')(1 - Z' - \varrho(R + \xi')), \\ \dot{w}' = -\mu w' + \kappa(R + \xi'), \\ \dot{Z}' = -\beta Z' + R + \xi', \end{cases} \quad (29)$$

where  $R$  satisfies the following relations:

$$\begin{aligned} R &= (\xi'^2 + v'^2 + w'^2)^{\frac{1}{2}} = (|X'|^2 + |Y'|^2)/2, \\ R + \xi &= |X'|^2, \quad R - \xi = |Y'|^2. \end{aligned}$$

Using projective system (29) it is convenient to study and visualize the dynamics of the initial system (4). For instance, it possible to demonstrate the presence of global stability, when conditions of Theorem 4 and condition (24) hold. Taking the same values of parameters  $\sigma = 4, r_1 = 5, r_2 = 0.001, e = -0.001, b = 5$ , considered for system (4) (see Fig. 3), one gets the same qualitative behavior in the phase space of system (29) (see Fig. 5).

As in the classical Lorenz system (1), for the complex Lorenz system (4) it is also known that the separatrix of saddle  $S_0$  can form a homoclinic loop, from which unstable cycles can arise and violate global stability (however, a set of measure zero does not affect the global attraction on a stationary set from a practical point of view). The following theorem provide the necessary condition for the existence of homoclinic orbits in the complex Lorenz system (4) (see [48–50]):

**Theorem 5.** *If conditions (24) are satisfied, then the necessary condition for the presence of a homoclinic orbit of the saddle equilibrium  $S_0$  is as follows:*

$$r_2 = \frac{e(1 - \sigma)}{2\sigma}. \quad (30)$$

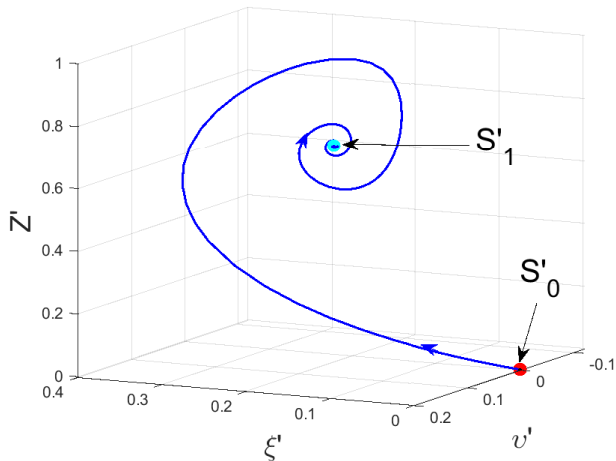


Figure 5: Global stability of the stationary set  $\{S'_0, S'_1\}$  in the projective system (29) with parameters  $\sigma = 4$ ,  $r_1 = 5$ ,  $r_2 = -e = 0.001$ ,  $b = 4$ .

**Corollary 1.** *For the "laser case", i.e., when  $e = -r_2$ , the homoclinic orbit can only be obtained if  $e = r_2 = 0$ .*

To prove condition (30), Vladimirov et al. considered the projective system (29), because unlike system (4), it has a 1-dimensional unstable manifold. The projections of unstable manifold  $W^u$  and stable manifold  $W^s$  in the space  $\mathcal{P}$ , i.e.  $\Pi(W^u)$  and  $\Pi(W^s)$ , can intersect only along the  $Z'$ -axis and a possible homoclinic orbit exists only if  $\kappa = 0$ , which coincides with condition (30).

For the parameters  $\sigma = 10$ ,  $r_2 = 4.5 \times 10^{-4}$ ,  $e = -0.001$ ,  $b = \frac{8}{3}$  of system (4), condition (30) is satisfied. In this case, system (4) has a unique equilibrium  $S_0$  (since  $e \neq -r_2$ ), and it is possible to find numerically the approximate value of such homoclinic bifurcation  $r_{1h} \approx 13.9$ , when two symmetric homoclinic orbits appear, forming a homoclinic butterfly (see Fig. 6). A further increase in the parameter  $r_1$  leads to the birth of two periodic saddle orbits from each homoclinic orbit. For the parameters  $\sigma = 10$ ,  $r_2 = 0$ ,  $e = 0$ ,  $b = \frac{8}{3}$ , condition (30) holds and system (4) has the following equilibrium points:  $S_0, S_\theta$  (since  $e = -r_2$ ), with  $r_{1h} \approx 13.9$ , system (4) has homoclinic orbits (see Fig. 7.)

Finally, let us mention the action of the projection map  $\Pi$  on various attractors in the space  $\mathcal{H}$ . In other words, preimages of different kinds of attractors in the original space  $\mathcal{H}$  and the corresponding images in the projection space  $\mathcal{P}$ . Basing on some geometrical properties of the map  $\Pi$ , in [48, 49] it is discussed that every limit set in  $\mathcal{H}/\mathcal{Z}$  can be represented locally (in a neighborhood of the given ray) by the direct product of a set in  $\mathcal{P}/\mathcal{Z}$  and the ray, i.e., the set  $\mathbb{R}^1$ . Here we exclude the sets of points  $\mathcal{Z}$  on the  $Z'$ -axes in phase spaces  $\mathcal{H}$  and  $\mathcal{P}$ , which are invariant with respect to systems (26) and (29), respectively. Moreover, the triplet  $(\mathcal{H}/\mathcal{Z}, \mathcal{P}/\mathcal{Z}, \Pi)$  forms a fiber bundle (see e.g. [51]),  $\Pi$  is continuous map and, thus, it maps connected/compact sets into connected/compact sets.

To illustrate this statement, let us list the following different types of attractors:

- (1) For the zero equilibrium  $S_0$  of system (26):  $\Pi(S_0) = S'_0$ , where  $S'_0 = (0, 0, 0, 0)$  is the zero equilibrium point of projective system (29);
- (2) For the circle of equilibria  $S_\theta$  of system (26):  $\Pi(S_\theta) = S'_1$ , where  $S'_1$  is an equilibrium point of system (29);
- (3) For limit cycle of system (26) the image is an equilibrium  $S'_1$  of system (29) in  $\mathcal{P}$ ;
- (4) For a torus of system (26) the image is a limit cycle of system (29) in  $\mathcal{P}$ ;
- (5) For a single homoclinic orbit of projective system (29) one has (as a preimage of map  $\Pi$ ) a continuum of homoclinic orbits in the original space  $\mathcal{H}$ , differing only by the common phase according to Eq. (28);
- (6) For a chaotic attractor of projective system (29) in  $\mathcal{P}$  one has (as a preimage) a chaotic attractor in  $\mathcal{H}$ ;
- (7) For a transient chaotic set of projective system (29) in  $\mathcal{P}$ , which collapses by colliding with stable equilibria or stable limit cycle, there exists (as a preimage) a transient chaotic set which after a certain time approaches eventually circle of equilibria  $S_\theta$  or a torus, respectively.

Summarizing the written above, further in our experiments we will examine the appearance of attractors in projective system (29), which has 1-dimensional unstable manifold of zero saddle equilibrium  $S'_0$  and use map (27) to get the corresponding preimages of the discovered attractors in the original system (4).

#### IV. OUTER ESTIMATION: THE ABSENCE OF TRIVIAL ATTRACTORS

System (4) possesses the absorbing set (defined by Eq. (6)) and for  $\sigma > b + 1$ ,  $r_1 > \max\{r'_{1c}, r'_{1c}\}$  (see Lemma 1 and 2) all equilibria are unstable. Further, in this article for the system (1) (and (8)) we will fix the classical values of parameters  $\sigma = 10$ ,  $b = \frac{8}{3}$  of real Lorenz model (1) and, following the "laser case", will specify two additional parameters:  $r_2 = -e = 0.001$ . For instance, when  $r_1 = 28 > r'_{1c}$ , it is possible to observe a self-excited chaotic attractor with respect to all equilibria of a stationary set (see Fig. 8). This gives an outer estimation of practical global stability.

#### V. THE BOUNDARY OF PRACTICAL STABILITY AND ABSENCE OF NONTRIVIAL ATTRACTORS

Inside the absorbing set, it is possible to study numerically the presence of nontrivial self-excited and hidden attractors for parameters  $r_1, \sigma, r_2, b$  not satisfying conditions (11) of global stability, i.e., by fixing  $\sigma, r_2, b$  and by decreasing  $r_1$  from  $r'_{1c}$ . For  $\sigma = 10$ ,  $r_2 = 0.001$ ,  $b = \frac{8}{3}$  this gives us the following region  $r_1 \in (r_{1gs}, r'_{1c})$ , where  $r_{1gs} \approx 1.96$  and  $r'_{1c} \approx 24.73$ .

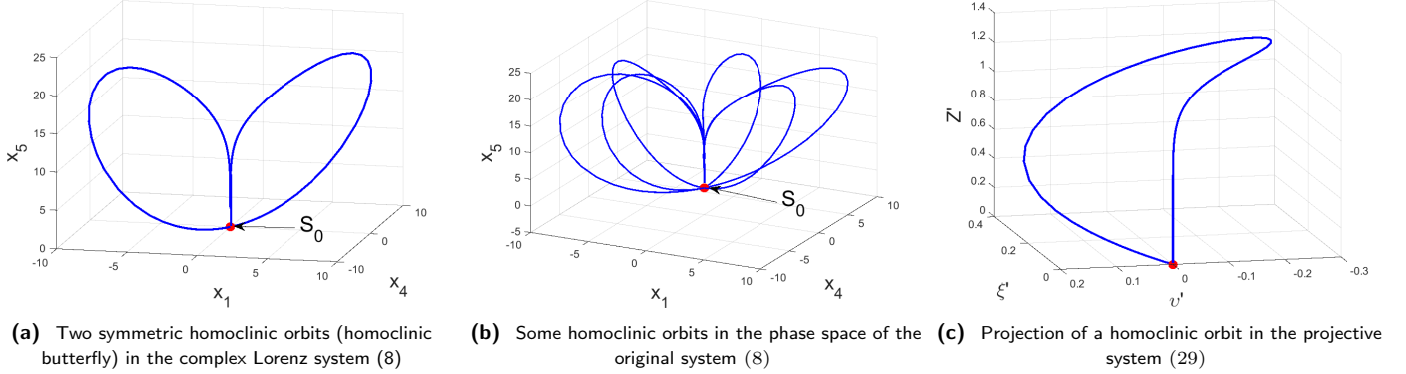


Figure 6: Visualization of homoclinic orbits with  $\sigma = 10, r_2 = 4.5 \times 10^{-4}, e = -0.001, b = \frac{8}{3}$  and  $r_{1h} \approx 13.9$ .

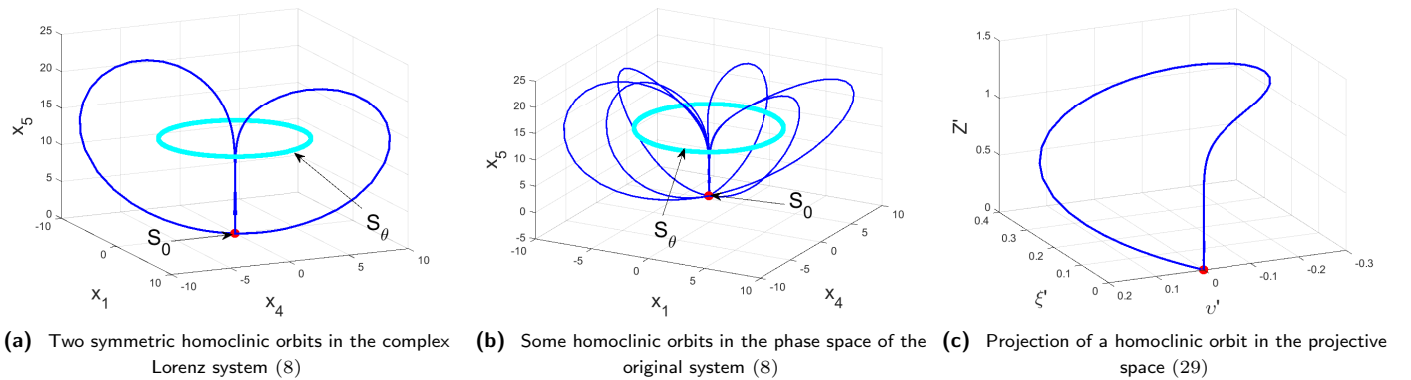


Figure 7: Visualization of homoclinic orbits with  $\sigma = 10, r_2 = 0, e = 0, b = \frac{8}{3}$  and  $r_{1h} \approx 13.9$ .

A nontrivial self-excited attractor can be observed numerically for  $24.09 \lesssim r_1 < r'_{1c} \approx 24.73$ . In this case of nontrivial multistability, system (8) possesses a local chaotic attractor  $\mathcal{A}$  which is self-excited with respect to equilibrium  $S_0$  and coexists with the set of trivial attractors  $S_\theta$  (see Fig. 9).

#### A. Hidden attractor or hidden transient set?

As we discussed above on the example of the classical Lorenz model (1), for a system possessing a transient chaotic set, the time of the transient process depends strongly on the choice of initial data in the phase space and also on the parameters of numerical solvers to integrate a trajectory (e.g., the order of the method, the step of integration, relative and absolute tolerances) [1]. This complicates the task of distinguishing a transient chaotic set from a sustained chaotic set (attractor) in numerical experiments.

Consider system (29), which represents the complex Lorenz system (4) in the projective space  $\mathcal{P}$ , with  $r_1 = 23.5, r_1 = 23.6$  and  $r_1 = 23.7$ . For a trajectory with a certain initial point, which is computed by a certain

solver with specific parameters, we estimate the moment of the end of transient behavior as the moment when the trajectory falls into a small vicinity of the stable equilibrium  $S'_1$ . Using MATLAB's standard procedure `ode45` with default parameters (relative tolerance  $10^{-3}$ , absolute tolerance  $10^{-6}$ ) for system (29) with parameters  $r_1 = 23.5, \sigma = 10, r_2 = -e = 0.001, b = \frac{8}{3}$  and for initial point  $u_0 = (0.5, 0.5, 0.5, 0.5)$ , a transient chaotic behavior is observed on the time interval  $[0, 1.78 \times 10^4]$ , for initial point  $u_0 = (0.4, 0.4, -0.3, 0.5)$  — on the time interval  $[0, 2.7 \times 10^4]$  and for initial point  $u_0 = (0.4, 0.4, 0.4, 0.4)$  — on the time interval  $[0, 4.6 \times 10^4]$ . If we slightly change the bifurcation parameter  $r_1$ , taking  $r_1 = 23.6$  and leaving all other parameters the same, and choosing initial point  $u_0 = (0.5, 0.5, 0.5, 0.5)$  a transient chaotic behavior is observed on the time interval  $[0, 3.49 \times 10^7]$ . For  $r_1 = 23.7$  with the same parameters and initial point a transient chaotic behavior continues over a time interval of more than  $[0, 10^8]$ . Thus, one can observe that a small increment of the bifurcation parameter  $r_1$  leads to a large increment of the time of transient process. For  $r_1 \in (23.7, 24.09)$ , it is a tough problem to estimate the time of transient process since the time for

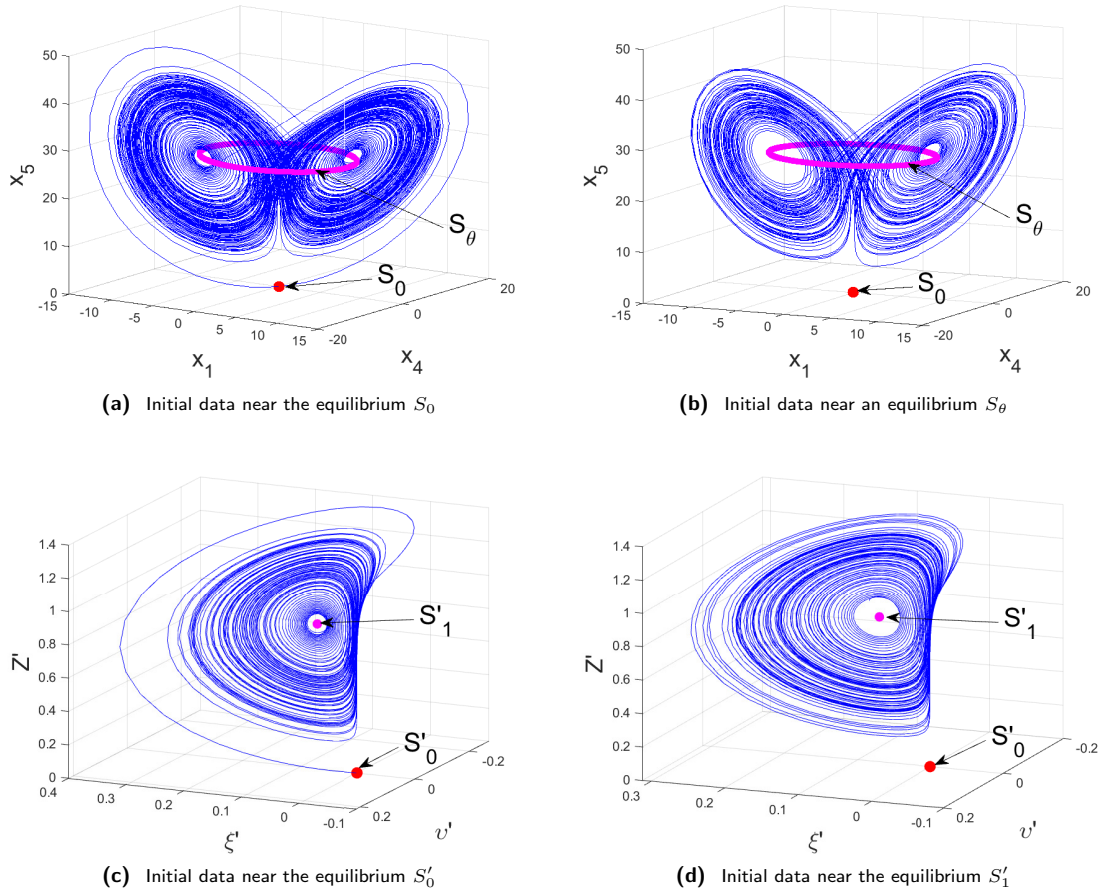


Figure 8: (a), (b) Numerical visualization of the self-excited chaotic attractor in system (8) with  $r_1 = 28$ ,  $\sigma = 10$ ,  $b = \frac{8}{3}$ ,  $r_2 = -e = 0.001$  by integrating the trajectories with initial data from small vicinities of the unstable equilibria  $S_0$ ,  $S_\theta$ ; (c), (d) The corresponding images in the projective space  $\mathcal{P}$ .

numerical integration is very large. Therefore, inside this interval of parameters for the particular trajectories it is hard to say whether the chaotic behavior is a long-hidden transient process, or a hidden sustained attractor. Note also that, if we consider parameters  $r_1 = 23.5$ ,  $\sigma = 10$ ,  $r_2 = -e = 0.001$ ,  $b = \frac{8}{3}$  with the same initial points and use `ode45` procedure with relative tolerance  $10^{-6}$ , for all these initial points the chaotic transient behavior will last over a time interval of more than  $[0, 10^7]$ , and corresponding transient chaotic sets won't collapse. To conclude this numerical study of transient chaotic behavior, we may suggest to specify precisely numerical solver, its parameters, initial data and time interval, along which the transient behavior continues.

Further in Appendices A-E, we study in detail the visualization of hidden transient chaotic sets in the complex Lorenz system in the form (8). We consider the "laser case", i.e.,  $e = -r_2$ , when system (8) has the equilibrium  $S_0$  and a circle of equilibria  $S_\theta$ . Two special techniques, i.e. numerical continuation method (NCM) and perpetual points method, are utilized to visualize hidden sets.

## VI. CONCLUSION

In this work, the complex Lorenz system, describing baroclinic instability in the atmosphere either the physics of detuned lasers, is considered. Analytical and numerical results demonstrate that the complex Lorenz system's dynamics is very rich, and, in comparison with the real Lorenz system, the loss of global stability may be connected with appearance of significantly different dynamical regimes. As for the Lorenz system, for the complex Lorenz system, on the one hand, it is demonstrated the possibility of using the apparatus of Lyapunov functions to estimate the boundary of global stability. On the other hand, it is shown that this problem is connected with the localization of sustained hidden chaotic attractors and their distinguishing from the hidden long-term transient chaotic sets. An attempt to study the problem of existence of sustained hidden chaotic attractor in the complex Lorenz system is made in the framework of a special analytical transformation, tacking into account the symmetry of the model.

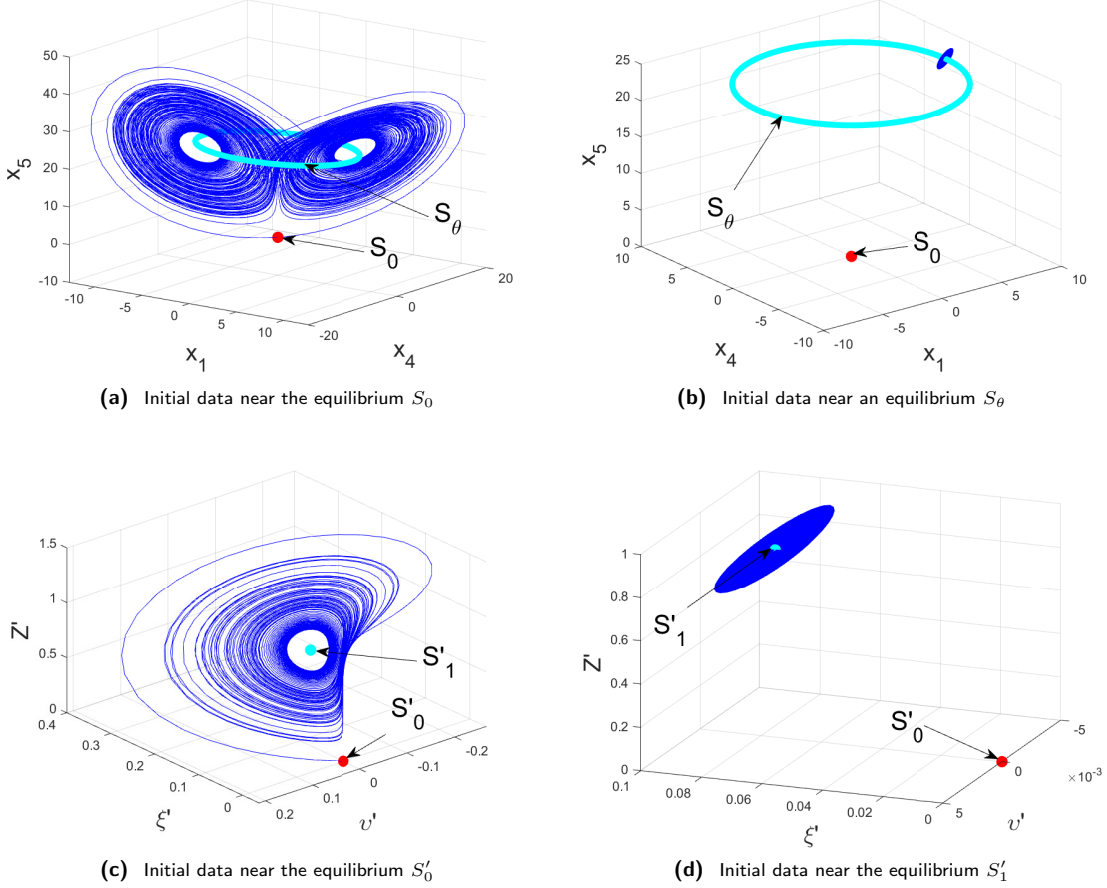


Figure 9: (a), (b) Numerical visualization of the self-excited local chaotic attractor in system (8) with  $r_1 = 24.6$ ,  $\sigma = 10$ ,  $b = \frac{8}{3}$ ,  $r_2 = -e = 0.001$  by a trajectory starting in the vicinity of the unstable equilibrium  $S_0$ . This attractor coexists with the stable set of equilibria  $S_\theta$ ; (c), (d) The corresponding images in the projective space  $\mathcal{P}$ .

## ACKNOWLEDGEMENT

This work is supported by the joint Grant from the Department of Science & Technology (DST, India) and the Russian Science Foundation (RSF, Russia) project 19-41-02002 (sects. I-IV) and by the General Administration of Missions (Ministry of Higher Education of Egypt).

- 
- [1] N. Kuznetsov, T. Mokaev, O. Kuznetsova, E. Kudryashova, The Lorenz system: hidden boundary of practical stability and the Lyapunov dimension, *Nonlinear Dynamics* 102 (2020) 713–732. doi:10.1007/s11071-020-05856-4.
- [2] M. Vidyasagar, *Nonlinear Systems Analysis*, Prentice-Hall, 1978.
- [3] W. Haddad, V. Chellaboina, *Nonlinear Dynamical Systems and Control: A Lyapunov-Based Approach*, Princeton University Press, 2011.
- [4] G. Leonov, V. Reitmann, V. Smirnova, *Nonlocal Methods for Pendulum-like Feedback Systems*, Teubner, Stuttgart-Leipzig, 1992.
- [5] V. Yakubovich, G. Leonov, A. Gelig, *Stability of Stationary Sets in Control Systems with Discontinuous Nonlinearities*, World Scientific, Singapore, 2004, [Transl from Russian: A.Kh. Gelig and G.A. Leonov and V.A. Yakubovich, Nauka, 1978].
- [6] E. Barbashin, N. Krasovskiy, On the stability of a motion in the large, *Dokl. Akad. Nauk SSSR* (In Russian) 86 (3) (1952) 453–456.
- [7] J. LaSalle, Some extensions of Liapunov’s second method, *IRE Transactions on circuit theory* 7 (4) (1960) 520–527.

- [8] G. Leonov, D. Ponomarenko, V. Smirnova, Frequency-Domain Methods for Nonlinear Analysis. Theory and Applications, World Scientific, Singapore, 1996.
- [9] N. Kuznetsov, M. Lobachev, M. Yuldashev, R. Yuldashev, E. Kudryashova, O. Kuznetsova, E. Rosenwasser, S. Abramovich, The birth of the global stability theory and the theory of hidden oscillations, in: 2020 European Control Conference Proceedings, 2020, pp. 769–774. doi:10.23919/ECC51009.2020.9143726.
- [10] J. LaSalle, S. Lefschetz, Stability by Liapunov's direct method: with applications, Academic Press, New-York-London, 1961.
- [11] V. Lakshmikantham, S. Leela, A. Martynyuk, Practical stability of nonlinear systems, World Scientific, 1990.
- [12] V. Aframovic, V. Bykov, L. Silnikov, On the origin and structure of the Lorenz attractor 234 (2) (1977) 336–339.
- [13] D. Auerbach, P. Cvitanović, J.-P. Eckmann, G. Gunaratne, I. Procaccia, Exploring chaotic motion through periodic orbits, Physical Review Letters 58 (23) (1987) 2387.
- [14] P. Cvitanović, Periodic orbits as the skeleton of classical and quantum chaos, Physica D: Nonlinear Phenomena 51 (1-3) (1991) 138–151.
- [15] L. P. Shilnikov, A. L. Shilnikov, D. V. Turaev, L. Chua, Methods of Qualitative Theory in Nonlinear Dynamics: Part 2, World Scientific, 2001.
- [16] G. Leonov, Shilnikov chaos in Lorenz-like systems, International Journal of Bifurcation and Chaos 23 (03), art. num. 1350058. doi:10.1142/S0218127413500582.
- [17] G. Leonov, N. Kuznetsov, T. Mokaev, Homoclinic orbits, and self-excited and hidden attractors in a Lorenz-like system describing convective fluid motion, The European Physical Journal Special Topics 224 (8) (2015) 1421–1458. doi:10.1140/epjst/e2015-02470-3.
- [18] G. Leonov, R. Mokaev, N. Kuznetsov, T. Mokaev, Homoclinic bifurcations and chaos in the Fishing principle for the Lorenz-like systems, International Journal of Bifurcation and Chaos 30, (https://doi.org/S0218127420501205). doi: S0218127420501205.
- [19] N. Levinson, Transformation theory of non-linear differential equations of the second order, Annals of Mathematics (1944) 723–737.
- [20] G. Leonov, N. Kuznetsov, V. Vagaitsev, Localization of hidden Chua's attractors, Physics Letters A 375 (23) (2011) 2230–2233. doi:10.1016/j.physleta.2011.04.037.
- [21] G. Leonov, N. Kuznetsov, Hidden attractors in dynamical systems. From hidden oscillations in Hilbert-Kolmogorov, Aizerman, and Kalman problems to hidden chaotic attractors in Chua circuits, International Journal of Bifurcation and Chaos in Applied Sciences and Engineering 23 (1), art. no. 1330002. doi:10.1142/S0218127413300024.
- [22] N. Kuznetsov, Hidden attractors in fundamental problems and engineering models. A short survey, Lecture Notes in Electrical Engineering 371 (2016) 13–25, (Plenary lecture at International Conference on Advanced Engineering Theory and Applications 2015). doi:10.1007/978-3-319-27247-4\_2.
- [23] N. Kuznetsov, Theory of hidden oscillations and stability of control systems, Journal of Computer and Systems Sciences International 59 (5) (2020) 647–668. doi:10.1134/S1064230720050093.
- [24] E. Lorenz, Deterministic nonperiodic flow, J. Atmos. Sci. 20 (2) (1963) 130–141.
- [25] G. Leonov, V. Boichenko, Lyapunov's direct method in the estimation of the Hausdorff dimension of attractors, Acta Applicandae Mathematicae 26 (1) (1992) 1–60.
- [26] G. Leonov, Lyapunov functions in the global analysis of chaotic systems, Ukr. Mat. Journal 70 (1) (2018) 40–62, (in Russian).
- [27] C. Sparrow, The Lorenz Equations: Bifurcations, Chaos, and Strange Attractors, Applied Mathematical Sciences, Springer New York, 1982.
- [28] Q. Yuan, F.-Y. Yang, L. Wang, A note on hidden transient chaos in the Lorenz system, International Journal of Nonlinear Sciences and Numerical Simulation 18 (5) (2017) 427–434.
- [29] B. Munmuangsaen, B. Srisuchinwong, A hidden chaotic attractor in the classical Lorenz system, Chaos, Solitons & Fractals 107 (2018) 61 – 66.
- [30] C. Grebogi, E. Ott, J. Yorke, Fractal basin boundaries, long-lived chaotic transients, and unstable-unstable pair bifurcation, Physical Review Letters 50 (13) (1983) 935–938.
- [31] Y. Lai, T. Tel, Transient Chaos: Complex Dynamics on Finite Time Scales, Springer, New York, 2011.
- [32] M.-F. Danca, N. Kuznetsov, Hidden chaotic sets in a Hopfield neural system, Chaos, Solitons & Fractals 103 (2017) 144–150. doi:https://doi.org/10.1016/j.chaos.2017.06.002.
- [33] G. Chen, N. Kuznetsov, G. Leonov, T. Mokaev, Hidden attractors on one path: Glukhovskiy-Dolzhanov, Lorenz, and Rabinovich systems, International Journal of Bifurcation and Chaos in Applied Sciences and Engineering 27 (8), art. num. 1750115.
- [34] J. Gibbon, M. McGuinness, The real and complex Lorenz equations in rotating fluids and lasers, Physica D: Nonlinear Phenomena 5 (1) (1982) 108–122.
- [35] A. Fowler, J. Gibbon, M. McGuinness, The complex Lorenz equations, Physica D: Nonlinear Phenomena 4 (2) (1982) 139–163.
- [36] A. Fowler, J. Gibbon, M. McGuinness, The real and complex Lorenz equations and their relevance to physical systems, Physica D: Nonlinear Phenomena 7 (1-3) (1983) 126–134.
- [37] C. Ning, H. Haken, Detuned lasers and the complex Lorenz equations: subcritical and supercritical hopf bifurcations, Physical Review A 41 (7) (1990) 3826.
- [38] Y. I. Neimark, P. S. Landa, Stochastic and Chaotic Oscillations, Kluwer Academic Publishers, Dordrecht, The Netherlands, 1992.
- [39] A. Rauh, L. Hannibal, N. Abraham, Global stability properties of the complex Lorenz model, Physica D: Nonlinear Phenomena 99 (1) (1996) 45–58.
- [40] G. Leonov, V. Reitmann, Attraktoreingrenzung für nichtlineare Systeme (in German), Teubner, 1987.
- [41] I. D. Chueshov, Introduction to the Theory of Infinite-Dimensional Dissipative Systems, ACTA Scientific Publishing House, Kharkov, 2002.
- [42] G. Leonov, On estimations of Hausdorff dimension of attractors, Vestnik St. Petersburg University: Mathematics 24 (3) (1991) 38–41, [Transl. from Russian: Vestnik Leningradskogo Universiteta. Matematika, 24(3), 1991, pp. 41–44].
- [43] N. Kuznetsov, T. Alexeeva, G. Leonov, Invariance of Lyapunov exponents and Lyapunov dimension for regular

- and irregular linearizations, *Nonlinear Dynamics* 85 (1) (2016) 195–201. doi:10.1007/s11071-016-2678-4.
- [44] N. Kuznetsov, The Lyapunov dimension and its estimation via the Leonov method, *Physics Letters A* 380 (25-26). doi:10.1016/j.physleta.2016.04.036.
- [45] G. Leonov, Lyapunov functions in the global analysis of chaotic systems, *Ukrainian Mathematical Journal* 70 (1) (2018) 42–66. doi:10.1007/s11253-018-1487-y.
- [46] E. Siminos, P. Cvitanović, Continuous symmetry reduction and return maps for high-dimensional flows, *Physica D: Nonlinear Phenomena* 240 (2) (2011) 187–198.
- [47] S. Froehlich, P. Cvitanović, Reduction of continuous symmetries of chaotic flows by the method of slices, *Communications in Nonlinear Science and Numerical Simulation* 17 (5) (2012) 2074–2084.
- [48] A. Vladimirov, V. Toronov, V. Derbov, On the complex Lorenz equations, in: *Proceedings of SPIE-The International Society for Optical Engineering*, 1997, pp. 97–106.
- [49] A. Vladimirov, V. Toronov, V. Derbov, The complex Lorenz model: Geometric structure, homoclinic bifurcation and one-dimensional map, *International Journal of Bifurcation and Chaos* 8 (04) (1998) 723–729.
- [50] A. Vladimirov, V. Toronov, V. Derbov, Properties of the phase space and bifurcations in the complex Lorenz model, *Technical Physics* 43 (8) (1998) 877–884.
- [51] S. Kobayashi, K. Nomizu, *Foundations of differential geometry*, Vol. 1,2, New York, London, 1963.
- [52] N. Kuznetsov, G. Leonov, T. Mokaev, A. Prasad, M. Shrimali, Finite-time Lyapunov dimension and hidden attractor of the Rabinovich system, *Nonlinear Dynamics* 92 (2) (2018) 267–285. doi:10.1007/s11071-018-4054-z.
- [53] G. Leonov, N. Kuznetsov, T. Mokaev, Hidden attractor and homoclinic orbit in Lorenz-like system describing convective fluid motion in rotating cavity, *Communications in Nonlinear Science and Numerical Simulation* 28 (2015) 166–174. doi:10.1016/j.cnsns.2015.04.007.
- [54] A. Prasad, Existence of perpetual points in nonlinear dynamical systems and its applications, *International Journal of Bifurcation and Chaos* 25 (2), art. num. 1530005.
- [55] D. Dudkowski, S. Jafari, T. Kapitaniak, N. Kuznetsov, G. Leonov, A. Prasad, Hidden attractors in dynamical systems, *Physics Reports* 637 (2016) 1–50. doi:10.1016/j.physrep.2016.05.002.
- [56] A. Prasad, A note on topological conjugacy for perpetual points, *International Journal of Nonlinear Science* 21 (1) (2016) 60–64.

### Appendix A: Localization via numerical continuation method

One of the effective methods for numerical localization of hidden attractors in multidimensional dynamical systems is based on the homotopy and numerical continuation method (NCM). It is based on the assumption that the position of the attractor changes continuously with the parameters changing. The idea is to construct a sequence of similar systems such that for the first (starting) system, the initial point for numerical computation of oscillating solution (starting attractor) can be obtained analytically. For example, it is often possible to consider the starting system with a self-excited starting attractor; then, the transformation of this starting attractor in the phase space is tracked numerically while passing from one system to another; the last system corresponds to the system in which a hidden attractor is searched [1, 52, 53].

In our experiment, we fix parameters  $\sigma, r_2, e, b$ , define parameters  $r_1 = 26.1 - \varepsilon$  and  $\sigma = \sigma^* = 10$ . For  $r_2 = 0.001$ ,  $e = -0.001$ ,  $b = 8/3$ ,  $\varepsilon = 0.7$ , we obtain  $r_1 = r_1^0 = 25.4$  and take  $P_0(r_1^0, \sigma^*)$  as the initial point of line segment on the plane  $(r_1, \sigma)$ . The eigenvalues of the Jacobian matrix at the equilibria  $S'_0, S'_1$  of system (29) for these parameters are the following:

$$\begin{aligned} S'_0 &: 2.00002, -0.1707, -0.7042, -0.7042, \\ S'_1 &: 0.0013 \pm 0.6238i, -0.8775, -0.7042. \end{aligned}$$

Consider on the plane  $(r_1, \sigma)$  a line segment, intersecting a boundary of stability domain of the equilibria  $S_\theta$  with the final point  $P_2(r_1^2, \sigma^*)$ , where  $r_1^2 = r_1^0 - 2\varepsilon = 24$ , i.e. the equilibrium  $S_\theta$  changes from saddle point to stable focus-node

$$\begin{aligned} S'_0 &: 2.00003, -0.1758, -0.7253, -0.7253 \\ S'_1 &: -0.0015 \pm 0.6257i, -0.8982, -0.7253. \end{aligned}$$

The initial point  $P_0(r_1^0, \sigma^*)$  corresponds to the parameters for which in the system (29), there exists a self-excited attractor. Then for the considered line segment, a sufficiently small partition step is chosen. At each iteration step of the procedure, an attractor in the phase space of the system (29) is computed. The last computed point at each step is used as the initial point for the computation at the next step. In this experiment, we use NCM with 3 steps on the path  $P_0(r_1^0, \sigma^*) \rightarrow P_1(r_1^1, \sigma^*) \rightarrow P_2(r_1^2, \sigma^*)$ , with  $r_1^1 = \frac{1}{2}(r_1^0 + r_1^2)$  (see Fig. 10). At the first step, we have a self-excited attractor with respect to unstable equilibria  $S_0$  and  $S_\theta$ ; at the second step, the equilibria  $S_\theta$  become stable, but the attractor remains self-excited with respect to equilibrium  $S_0$ ; at the third step, it is possible to visualize a hidden chaotic set of system (29) (see Fig. 11). In Fig. 12 visualizations of the hidden chaotic set in both initial space  $\mathcal{H}$  and projective space  $\mathcal{P}$  are depicted.

For  $\sigma = 10, r_1 = 24, r_2 = 0.002, e = -0.001, b = \frac{8}{3}$ , here the parameter  $r_2$  is slightly different from that in the above case and  $e \neq -r_2$ . Therefore  $S_0$  is the only

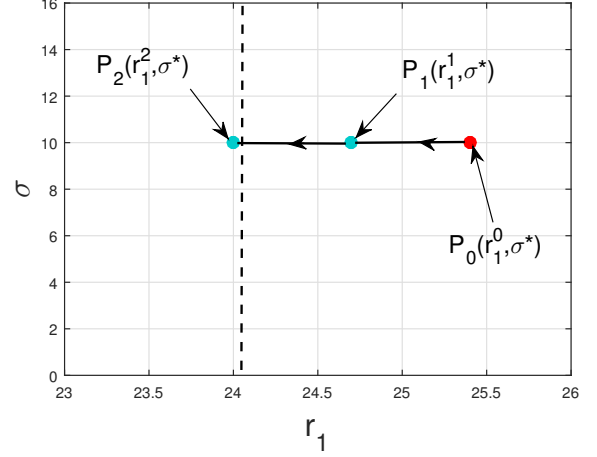


Figure 10: Path  $P_0(r_1^0, \sigma^*) \rightarrow P_1(r_1^1, \sigma^*) \rightarrow P_2(r_1^2, \sigma^*)$ , in parameters plane  $(r_1, \sigma)$  for the localization of hidden chaotic set in system (29) with  $r_2 = 0.001$ ,  $e = -0.001$ ,  $b = \frac{8}{3}$ . Here  $r_1^0 = 25.4, r_1^1 = 24.7, r_1^2 = 24, \sigma = \sigma^* = 10$ ;

- (●)  $P_0(r_1^0, \sigma^*)$  : self-excited attractor w.r.t.  $S'_{0,1}$ ;
- (●)  $P_1(r_1^1, \sigma^*)$  : self-excited attractor w.r.t.  $S'_0$ ;
- (●)  $P_2(r_1^2, \sigma^*)$  : hidden chaotic set.

equilibria of the system (8). In this case, we can also visualize a hidden chaotic set in the system (8). To verify that the set in Fig. 13b is hidden, around equilibrium  $S_0$ , we choose a small spherical vicinity of radius  $\delta = 0.2$  and take  $N$  random initial points on it (in our experiment,  $N = 100$  as in Fig. 14b). Using MATLAB, we integrate system (8) with these initial points to explore the obtained trajectories. We repeat this procedure several times in order to get different initial points for trajectories on the sphere. We get the following results: all the obtained trajectories tend to the torus and do not tend to the chaotic set (see Fig. 14a), this torus is closer<sup>5</sup> to the set of equilibria  $S_\theta$  (see Fig. 13a). This gives us a reason to classify the chaotic set, obtained in the system (8), as the hidden one (see Fig. 13b).

<sup>5</sup> The distance between the torus and the equilibria  $S_\theta$  can be estimated by considering the last point on torus and plane, which contains the set of equilibria  $S_\theta$ . If we consider in  $\mathbb{R}^5$  the point  $P(x_1^*, x_2^*, x_3^*, x_4^*, x_5^*)$  and the plane  $A(x_1 - x_{01}) + B(x_2 - x_{02}) + C(x_3 - x_{03}) + D(x_4 - x_{04}) + E(x_5 - x_{05}) = 0$ , then the distance from the point  $P$  to the plane is:

$$d = \frac{|Ax_1^* + Bx_2^* + Cx_3^* + Dx_4^* + Ex_5^* + F|}{\sqrt{A^2 + B^2 + C^2 + D^2 + E^2}}.$$

To determine the equation of a plane in  $\mathbb{R}^5$  one can consider five points, which do not lie on the same straight line. The normal vector to a plane can be obtained by taking the cross product of four vectors on this plane. In our case equation of the plane which contains the set of equilibria  $S_\theta$  is:  $x_5 - 23 = 0$ . From Fig. 13a the last point on the torus is  $P(-2.5011, 7.6357, -2.5958, 7.9228, 22.8110)$ , then the distance from this point to the plane  $x_5 - 23 = 0$  is:  $d = 0.1890$ .

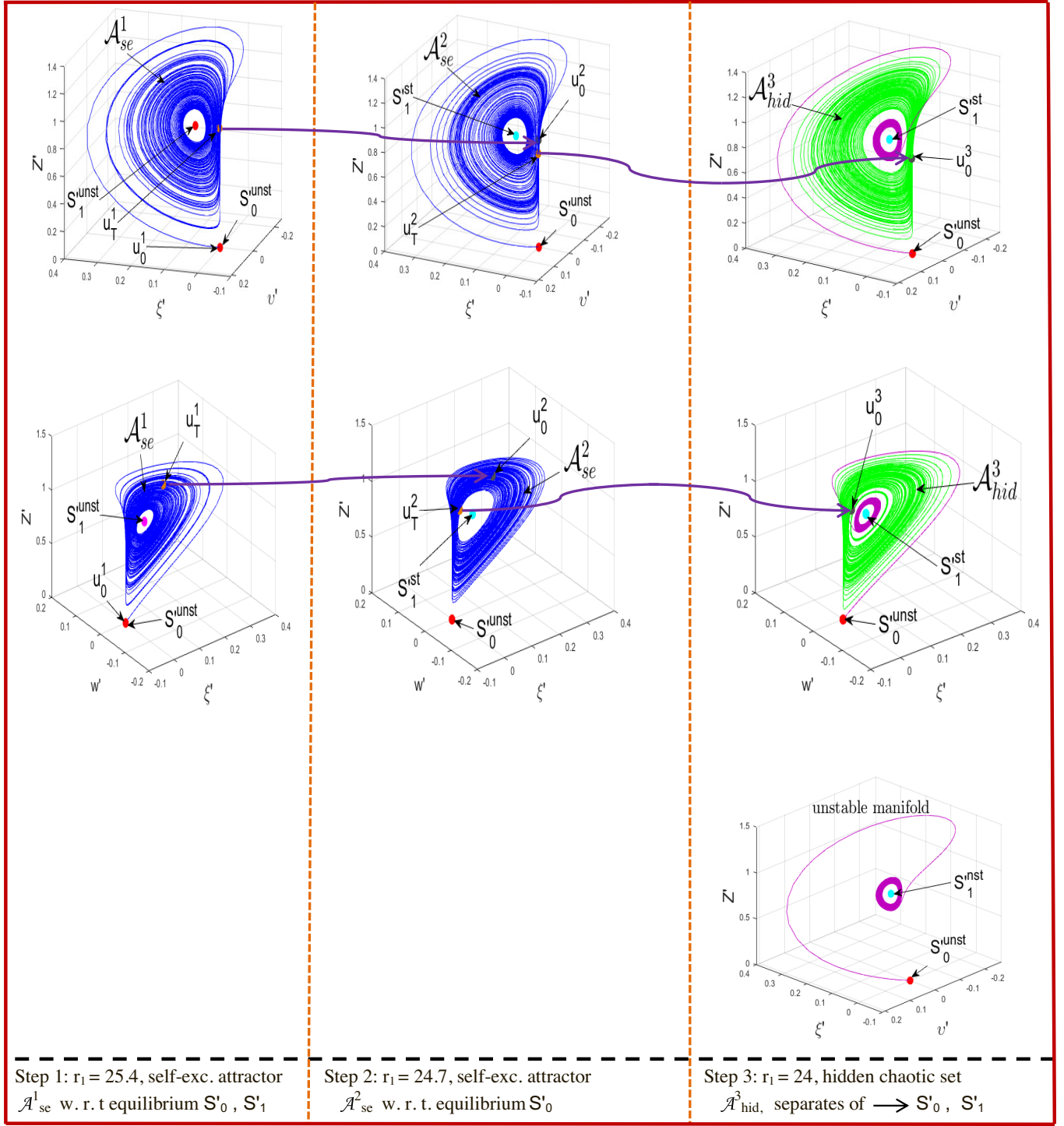


Figure 11: Localization, by NCM, of hidden chaotic set in system (29) with  $(\sigma, r_1, r_2, e, b) = (10, 24, 0.001, -0.001, \frac{8}{3})$ . Trajectories  $u^i(t) = (x_1, x_2, x_3, x_4, x_5)$  (blue and green) are defined on the time interval  $[0, T = 10^3]$ , and initial point (gray) on  $(i + 1)$ -th iteration is defined as  $u_0^{i+1} := u_T^i$  (violet arrows), where  $u_T^i = u^i(T)$  is a final point (orange).

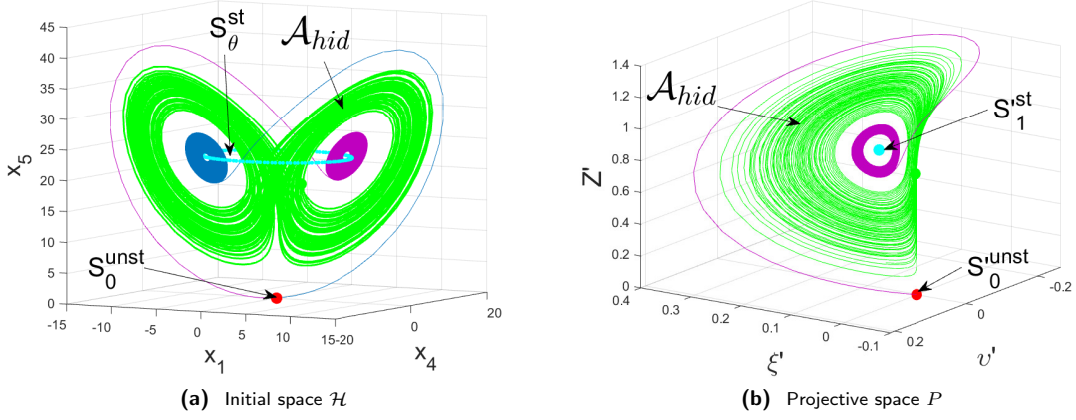


Figure 12: Localization of hidden chaotic set in system (8) and the corresponding image in system (29) for  $(\sigma, r_1, r_2, e, b) = (10, 24, 0.001, -0.001, 8/3)$ .

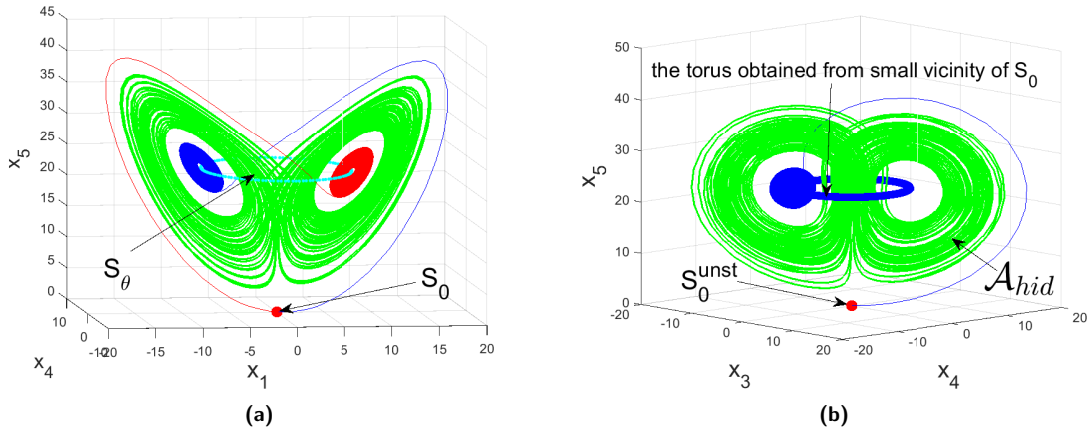


Figure 13: (a) A trajectory that attracts to a torus (blue) in the time interval  $[0, 7000]$ , which is closer to the equilibria  $S_\theta$  (magenta) (b) Visualization of a hidden chaotic set in system (8) with time interval  $[0, 100]$ ,  $(\sigma, r_1, r_2, e, b) = (10, 24, 0.002, -0.001, \frac{8}{3})$  and the initial point is  $(5, 5, 5, 5, 5)$ .

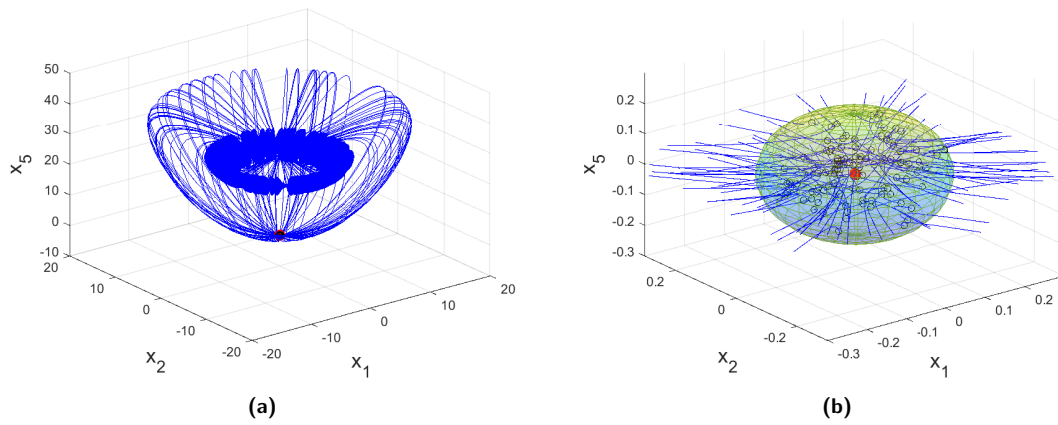


Figure 14: (a) Visualization of trajectories that tend to the torus in the time interval  $[0, 7000]$ , with starting points from a spherical of random points in a vicinity of  $S_0$ ; (b) Magnification of the area around  $S_0$  to show the spherical of random points and the considered 100 trajectories that tend to the torus.

## Appendix B: Localization using perpetual points

Consider system (8) as an autonomous differential equation of general form:

$$\dot{u} = f(u), \quad (\text{B1})$$

where  $u = (x_1, x_2, x_3, x_4, x_5) \in \mathbb{R}^5$  represents the right-hand side of system (8).

The equilibrium points of a dynamical system are the ones at which the velocity and acceleration of the system simultaneously become zero. In this subsection, we state that there are points, termed as perpetual points [54], which may help to visualize hidden attractors.

For system (B1), the equilibrium points  $u_{ep}$  are defined by the equation  $\dot{u} = f(u_{ep}) = 0$ . Consider a derivative of system (B1) with respect to time:

$$\ddot{u} = J(u)f(u) = g(u), \quad (\text{B2})$$

where  $J(u) = \left[ \frac{\partial f_i(u)}{\partial u_j} \right]_{i,j=1}^5$  is the Jacobian matrix. Here,  $g(u)$  may be termed as an acceleration vector. System (B2) shows the variation of acceleration in the phase space. Similar to the equilibrium points estimation, where we set the velocity vector to zero, we can also get a set of points, where  $\ddot{u} = g(u_{pp}) = 0$  in (B2), i.e. the points corresponding to the zero acceleration. At these points, the velocity  $\dot{u}$  may be either zero or nonzero. This set includes the equilibrium points  $u_{ep}$  with zero velocity as well as a subset of points with nonzero velocity. These nonzero velocity points  $u_{pp}$  are termed as perpetual points [54–56].

**Remark 4.** *The analytical formula of the perpetual points of system (8) can not be derived, meanwhile the numerical solution of the algebraic system  $\ddot{u} = g(u_{pp}) = 0$  is  $x_1 = x_2 = x_3 = x_4 = x_5 = 0$ , which coincide with the equilibrium  $S_0$ , so system (8) has no perpetual points. For system (29), which structure seems simpler than the original system (8),  $x'_1 = x'_2 = x'_3 = x'_4 = x'_5 = 0$  is the only solution of the system  $\ddot{u} = g(u_{pp}) = 0$ , thus, there are also no nonzero velocity points  $u_{pp}$ .*

## Appendix C: Numerical verification of basins of attraction near the zero equilibrium point

For the system (8) the eigenvalues at  $S_0$  are:  $10.6323 \pm 0.0003i$ ,  $-21.6323 \pm 0.0007i$ ,  $-2.6667$ . So the equilibria  $S_0$  has 2-dimensional unstable manifold. For the first two eigenvalues  $\lambda_{1,2} = 10.6323 \pm 0.0003i$  with positive real part, the corresponding eigenvectors are:  $v_1 = (-0.3084, -0.3084i, -0.6363, -0.6363i, 0)$  and  $v_2 = (-0.3084, 0.3084i, -0.6363, 0.6363i, 0)$  respectively. In the case of complex eigenvalues we can use the following formula to plot trajectories in a vicinity of  $S_0$

$$u(t) = \Omega e^{\alpha t} [\eta \sin(\beta t + \delta) + \mu \cos(\beta t + \delta)], \quad (\text{C1})$$

where  $\Omega$  is a constant that represent the size of the vicinity and should be small,  $\alpha$ ,  $\beta$  are real and imaginary parts of the eigenvalues respectively,  $\delta$  is an auxiliary angle,  $\eta = \text{Re } v_1$  and  $\mu = \text{Im } v_1$ . Initial points of unstable manifolds of  $S_0$  can be obtained by putting  $t = 0$  in Eq. (C1) as

$$u(0) = \Omega [\eta \sin(\delta) + \mu \cos(\delta)], \quad (\text{C2})$$

In Fig. 15 we plotted local stable, unstable manifolds of  $S_0$  and random initial points on local 2-D unstable manifolds of  $S_0$ . Fig. 16 shows unstable manifolds with random initial points from local 2-D unstable manifolds of  $S_0$  (in our experiment, we choose 100 random points for the angle  $\delta$  inside interval  $(0, 2\pi)$  and fix the size of vicinity as  $\Omega = 0.5$ . We repeat this procedure several times in order to get different initial points). From Fig. 16 one can see that, these unstable manifolds form by their scrolling a tube around the circle of equilibria  $S_\theta$ . This experiment confirms that all trajectories which start from a vicinity of the unstable equilibria  $S_0$  go to the circle of equilibria  $S_\theta$ , and this means that the green set in Fig. 12a is not self-excited. We can do the same experiment in the case of the torus as in Fig 13b. In Fig. 17 we plotted trajectories with random initial points on local 2-D unstable manifolds of  $S_0$ , which tend to the torus. So the green set in Fig 13b is not self-excited. In order to demonstrate separation between basins of attraction of  $S_\theta$  and the green set (as in Fig. 12a) which is located between the blue tube that is formed by scrolling of these trajectories and the domain which is defined by separatrixes. We need not only to separate basin of attraction of this green set from these blue manifolds, but also from trajectory going from infinity to  $S_0$  which can be derived analytically by formula  $u(t) = (0, 0, 0, 0, z_0 \exp(-bt))$ ,  $z_0 \in \mathbb{R}$ . Because of the system (8) is 5-dimensional it is difficult to show such separation, so we can say that the green set it is possible to be an attractor.

## Appendix D: Numerical verification of basins of attraction around the set of equilibria

In order to numerically verify the attractiveness of the chaotic set the following numerical experiment can be used. In this experiment, we consider initial points on the various line segments in the vicinity around the set of equilibria  $S_\theta$  in Figs. 12a and 13b (see Fig. 18). From Fig. 18 we can conclude the following: around the equilibria  $S_\theta$  there is a vicinity such that trajectories starting from this vicinity approach equilibria  $S_\theta$  and outside it approach attractor. For Fig. 13b the vertical and horizontal diagonals are considered with radius 2.5 and 2 respectively and partition step 0.01. And for the others line segments as in Figs. 18b and 18c we used the same partition step. In Fig. 19 we plotted two trajectories with initial points from blue and red parts of vertical diagonal. The same procedure can be used for Fig. 12a with vertical and horizontal diagonals

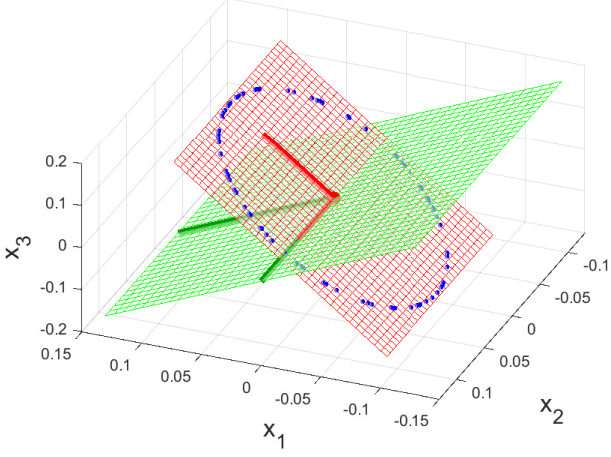


Figure 15: Visualization of local stable, unstable manifolds of  $S_0$  and random initial points on local 2-D unstable manifolds of  $S_0$ . (Red) local 2-D unstable manifold corresponding to  $\lambda_{1,2} = 10.6323 \pm 0.0003i$ , (Green) local 2-D stable submanifold corresponding to  $\lambda_{3,4} = 21.6323 \pm 0.0007i$ .

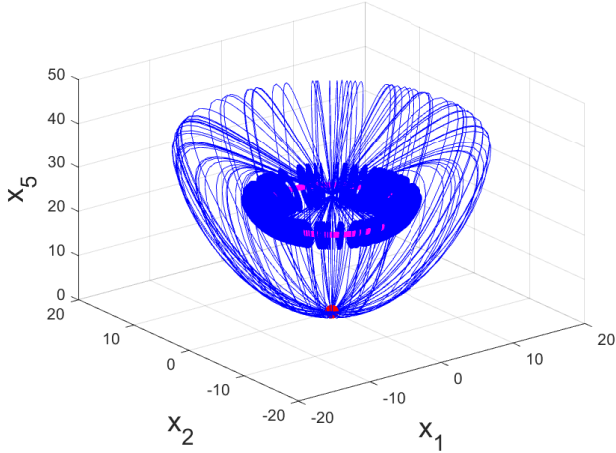


Figure 16: Visualization of unstable manifolds in system (8) with  $\sigma = 10$ ,  $r_1 = 24$ ,  $r_2 = -e = 0.001$ ,  $b = \frac{8}{3}$  and 100 random initial points in a vicinity of  $S_0$ , that tend to the circle of equilibria  $S_\theta$ .

have radius 3 and 2.5 respectively and partition step 0.01 on all considered line segments. Fig. 20 shows two trajectories with starting points from blue and red parts of vertical diagonal. In addition, another procedure can be used to verify that the green set in Fig. 12a not fall on the circle of equilibria  $S_\theta$ . Around one scroll of trajectory of an unstable manifold from its outer sides we consider line segments with length 5 and partition step 0.01 as in Fig. 21a. In Fig. 21b we plotted a trajectory with starting point from the upper outer line segment.

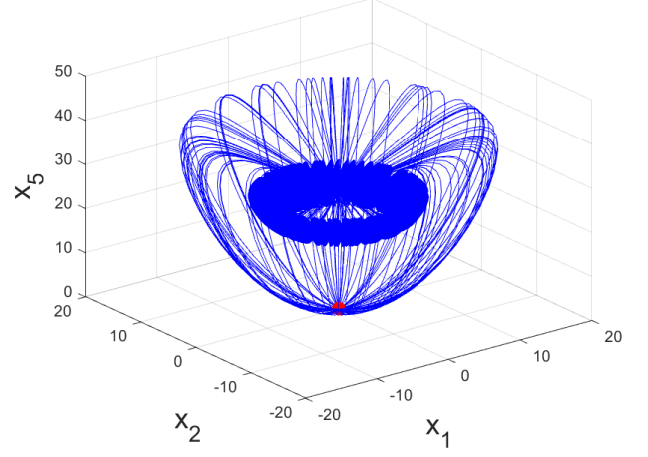


Figure 17: Visualization of trajectories in the time interval  $[0, 7000]$  with in system (8) with  $\sigma = 10$ ,  $r_1 = 24$ ,  $r_2 = 0.002$ ,  $e = -0.001$ ,  $b = \frac{8}{3}$  and 100 random initial points in a vicinity of  $S_0$  tending to the torus.

#### Appendix E: Attempts to prove the attractiveness of the transient set

To demonstrate strictly the attractiveness of the green sets as in Figs. 12a and 13b, another technique can be utilized. The idea of this technique is based on the fact that the complex Lorenz system (4) has a projective space, in which the states differing only by a common phase of variables  $X$  and  $Y$  are considered to be equivalent (see Section III).

Now, it is important to mention the following properties of the projective system (29) [48, 49]:

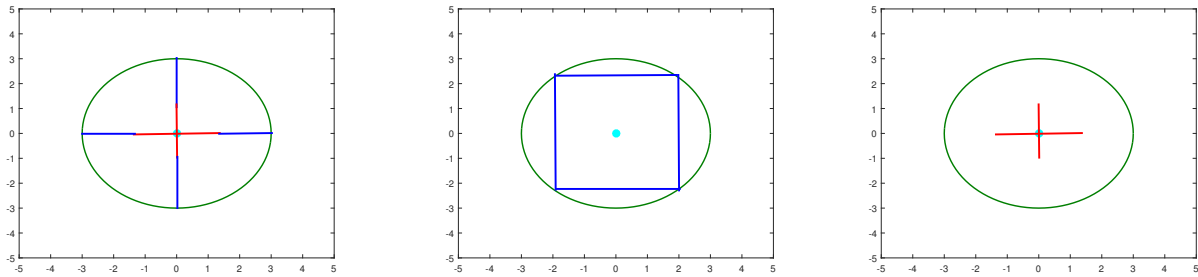
- (i) All physical information and dynamics in the phase space of the system (4) can be derived from the equations of motion (29) in the projective space.
- (ii) The projective system (29) has a 1-dimensional unstable manifold and 3-dimensional stable manifold.

Note that the projective system (29) has the following two equilibria:  $S'_0 = (0, 0, 0, 0)$  and  $S'_1 = (\xi'_1, v'_1, w'_1, Z'_1)$ , where

$$\xi'_1 = \frac{\beta(\mu^2 + \kappa^2)(\mu^2 - \kappa^2)}{2\mu^4(\beta\varrho + 1)}, \quad v'_1 = 0, \quad w'_1 = \frac{\beta v(\mu^2 + \kappa^2)}{\mu^3(\beta\varrho + 1)}, \quad Z'_1 = \frac{\mu^2 + \kappa^2}{\mu^2(\beta\varrho + 1)}.$$

The equilibria  $S'_0$  and  $S'_1$  in the projective space represent the projections of the equilibria  $S_0$  and  $S_\theta$  of the system (8) respectively. For the torus as in Fig. 13a its projection in the projective space  $\mathcal{P}$  is a limit cycle  $\Gamma$ .

Because of the projection system (29) has a 1-dimensional unstable manifold and the projective mapping (27) preserves the "chaoticity" of attractors. So, it is reasonable to use the projection system (29) to identify whether the chaotic sets in Figs. 12a and 13b are



(a) The starting trajectories from all points lie on blue parts and red parts of these diagonals approach attractor and equilibria respectively  
 (b) The starting trajectories from all points lie on these blue line segments approach attractor  
 (c) The starting trajectories from all points lie on these red line segments approach equilibria

Figure 18: Visualization of the white region around the set of equilibria  $S_\theta$  in Figs. 13 and 12a and the considered line segments.

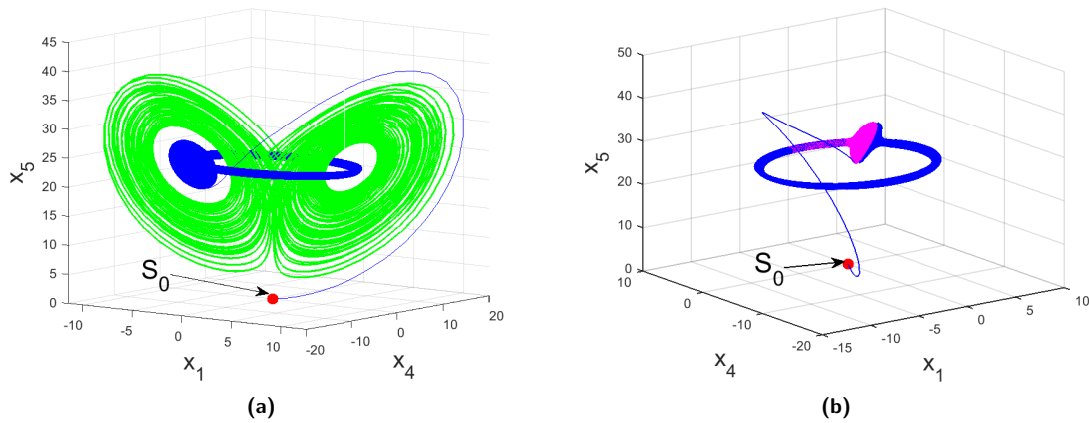


Figure 19: Visualization of two trajectories with initial points from blue and red parts of vertical diagonal in the white gap of Fig. 13.

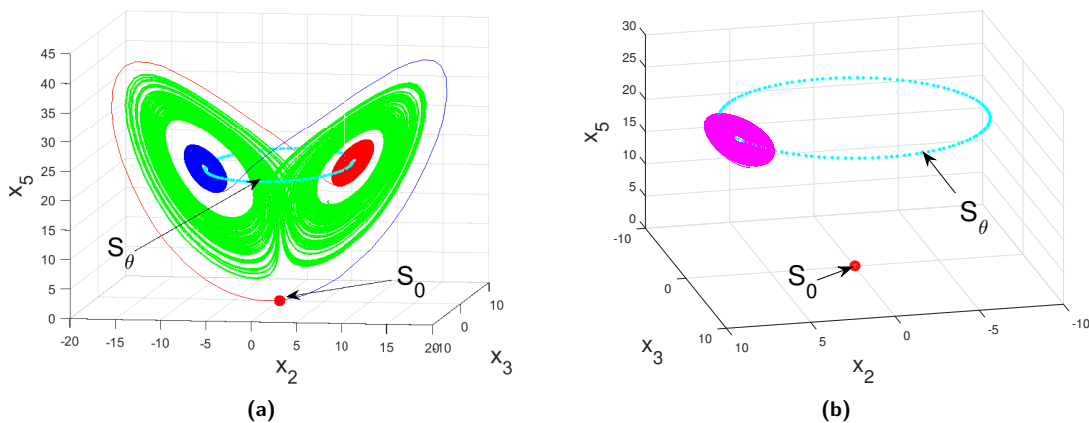


Figure 20: Visualization of two trajectories with initial points from blue and red parts of vertical diagonal in the white gap of Fig.12a.

attractors or transient chaotic sets. For the parameters  $\sigma = 10, r_1 = 24, r_2 = 0.001, e = -0.001, b = \frac{8}{3}$  (see

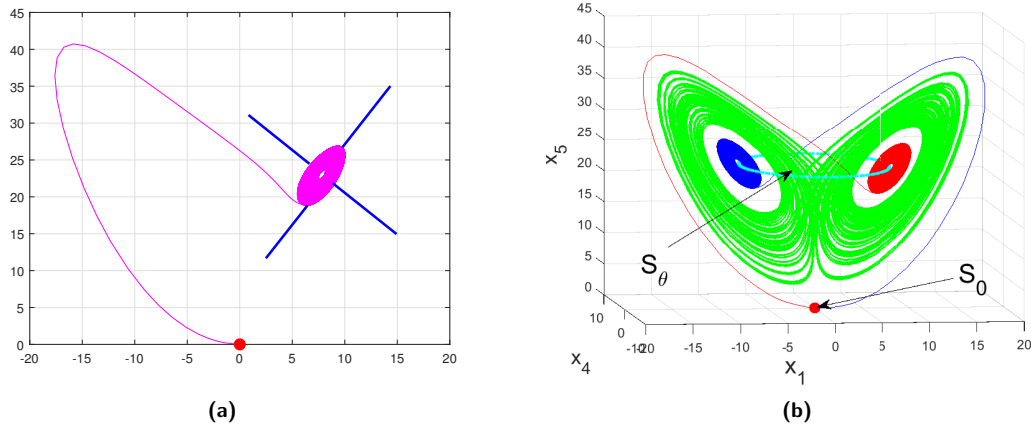


Figure 21: (a) Visualization of line segments around the unstable manifold in Fig. 13, starting trajectories from all points on these line segments approach attractor; (b) Localization of a trajectory with initial point on the upper outer line segment.

Fig. 12a), around the equilibria  $S'_0$  we choose a small spherical vicinity of radius 0.002 and consider 100 random initial points on it. From Fig. 22 one can observe the following: all the considered unstable manifolds of  $S'_0$

go in one direction and approach  $S'_1$ . We did the same experiment for the case of the torus and got the same conclusion (see Fig. 23).

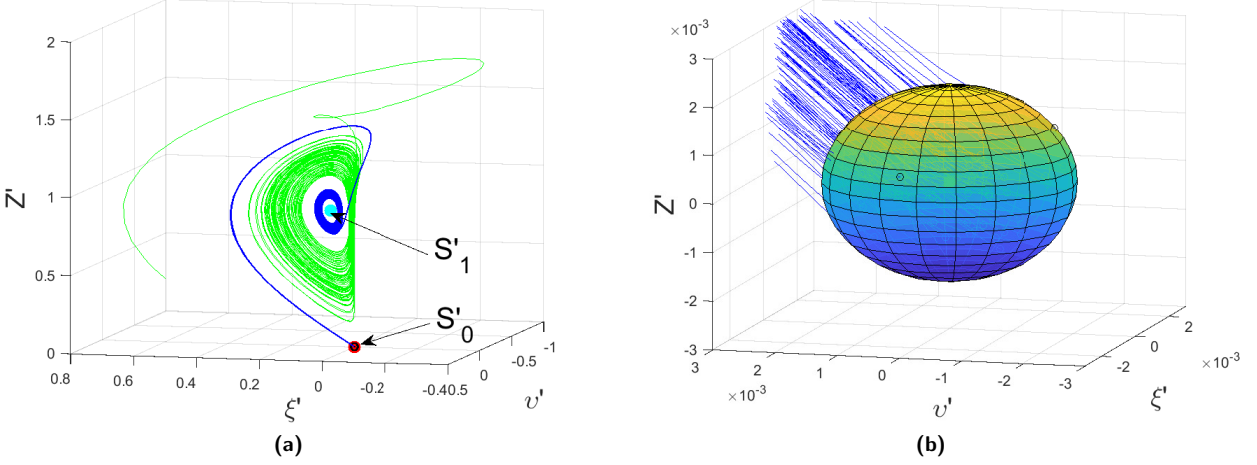


Figure 22: (a) Localization of the chaotic set (green) in the projective space and 100 unstable manifolds with starting points from a spherical of random points in a vicinity of  $S'_0$ , with  $(\sigma, r_1, r_2, e, b) = (10, 24, 0.001, -0.001, \frac{8}{3})$ ; (b) Magnification of the area around  $S'_0$  to show the sphere of random initial points and the corresponding 100 trajectories tending to  $S'_1$ .

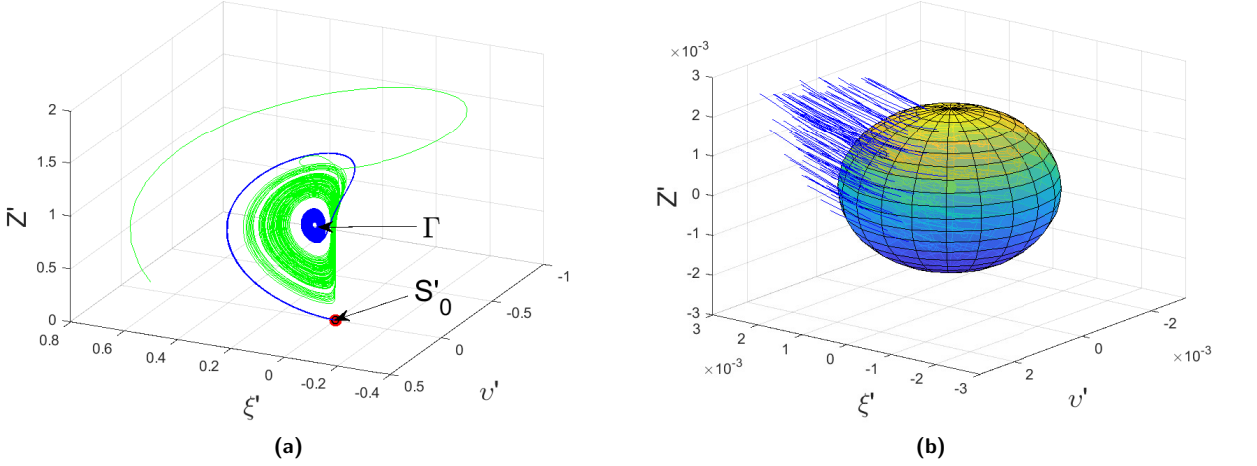


Figure 23: (a) Localization of the chaotic set (green) in the projective space and 100 unstable manifolds with starting points from a spherical of random points in a vicinity of  $S'_0$ , with  $(\sigma, r_1, r_2, e, b) = (10, 24, 0.002, -0.001, \frac{8}{3})$ ; (b) Magnification of the area around  $S'_0$  to show the spherical of random points and the considered 100 trajectories tending to the limit cycle  $\Gamma$ .